Effect of impingement surface roughness on the noise from impinging jets

Abhijit Dhamanekar and K. Srinivasan

Citation: Physics of Fluids (1994-present) **26**, 036101 (2014); doi: 10.1063/1.4866977
View online: http://dx.doi.org/10.1063/1.4866977
View Table of Contents: http://scitation.aip.org/content/aip/journal/pof2/26/3?ver=pdfcov
Published by the AIP Publishing

PHYSICS OF FLUIDS **26**, 036101 (2014)

Effect of impingement surface roughness on the noise from impinging jets

Abhijit Dhamanekar and K. Srinivasan[a)]
Department of Mechanical Engineering, Indian Institute of Technology Madras, Chennai 600036, India

(Received 19 July 2013; accepted 22 January 2014; published online 10 March 2014)

This paper presents extensive acoustic measurements on jets impinging on surfaces of various surface roughness values. Besides surface roughness, the effects of nozzle-to-plate spacing distance and nozzle pressure ratio are also investigated. Turbulent mixing noise and tonal noise are explained using far-field wall-jet velocity and impingement region temperature fields. The results demonstrate that roughness of the impingement plate widens the staging region of impingement noise. In general, high speed jet impinging on a rough plate generates less noise compared to a smooth plate. When tones are removed from the spectra, it is found that acoustic power monotonically decreases with increasing surface roughness. Thermal imaging in the stagnation region indicates that whenever tones are present, the temperature at the stagnation region is high. Further, sound pressure directivity pattern of impingement noise is constructed by superimposing a wall-jet and a free jet in the appropriate orientations. © *2014 AIP Publishing LLC*. [http://dx.doi.org/10.1063/1.4866977]

I. INTRODUCTION

Impinging jets are ubiquitous in mechanical, aerospace, and process industry. Applications range from impingement cooling, atomization, manufacturing processes to rockets and V/STOL aircraft. In some of these applications, noise is a serious concern. For instance, launch pads of aircraft or V/STOL aircraft are acoustically hazardous, posing health issues to operating personnel. V/STOL generates lifting force by vertical air jet impinging on ground using nozzles and lifting fans. These supersonic highly energetic jets generate significant static pressure and thermal load on the aircraft carrier platform. The jets may also impinge on the ground and cause flow around the aircraft resulting in lift reduction, thrust loss, ingestion of hot gas through engine air intakes and combustion instabilities. Such problems have attracted the researchers from 1930s not only due to their applications but also for the interesting physics involved. A brief survey of the literature in the areas of impinging tonal noise and turbulent boundary layer noise is presented below.

A. Impingement tones

According to Powell,[1] Konig[2] was perhaps the first one to report tonal noise from impinging jets. Powell[1,3] and Curle[4] suggested feedback theory for the generation of tonal noise. Marsh[5] observed that the overall sound power output increases rapidly with decrease of nozzle to plate separation distance for subsonic impinging jets. The spectrum of noise is modified as separation distance increases; frequency and amplitude of the dominant tone decreases and the sharp peak transforms into a broadband-like hump. Mørch[6] and Henderson[7] carried out experiments on impinging jet for various conditions and found Hartmann type of oscillations responsible for intense noise under certain operating conditions. Wagner[8] showed using flash shadowgraph technique that acoustic tone frequency is the same as that of very large ring vortices moving along the jet. Nakatogawa

[a)]Life Member, APS. Author to whom correspondence should be addressed, Electronic mail: ksri@iitm.ac.in. Tel.: +91 (44) 2257-4703. Fax: +91 (44) 2257-4652.

et al.[9] studied impinging jets with reflector plate placed behind the nozzle. They observed standoff shock oscillations when the plate was present in the decelerating region of the jet. Gubanova *et al.*[10] observed a reverse flow towards the stagnation point and hence confirmed the appearance of stagnation bubble for some cases. Neuwerth[11] observed the generation of discrete screech frequencies in choked underexpanded jet and related them to the feedback between the flow and the acoustic pressure field. In the case of choked impinging jet, the acoustic emission is dominant when there are less than five shock cells between the nozzle exit and the obstacle. He investigated feedback mechanism for this case and the discrete frequencies were determined as a function of nozzle-obstacle spacing, nozzle diameter, and reservoir pressure. Semiletenko *et al.*[12] focused on shock oscillations and found that oscillations disappear when there is enough space for accommodating the second compression shock in front of plate. Petrie[13] investigated the acoustic power of impinging jets on flat, concave, and convex surfaces. Ho and Nosseir[14] carried out impinging jet experiments by varying Mach number and nozzle to plate spacing. Their detailed investigation revealed staging of acoustic power. Powell[15] measured the flow and acoustic parameters as well as visualized the flow of underexpanded jet impinging on plates of various sizes, nozzle-plate spacing, and jet pressure ratios. He found three instabilities: (i) high-harmonic shock oscillations like Hartmann's resonator for small plates, (ii) acoustic feedback involving instability for large plates, and (iii) random cases when large plates are placed very near the nozzle. Norum[16] identified four different regions (based on nozzle-to-plate spacing) of tone generation with different frequency characteristics.

Donaldson and Snedeker[17] extensively investigated axisymmetric jets impinging on various surfaces. They reported a steeper radial velocity gradient at the stagnation point for oblique impingement than that for normal impingement. The underexpanded jet impingement results in two types of flow field near the wall depending on the jet core and nozzle-impinging surface spacing. First case is when the jet core length is greater than nozzle-plate spacing, i.e., obstacle is within the supersonic cell structure, a normal shock forms ahead of the plate. Second case is when the obstacle is outside the jet core, the flow field is similar to the subsonic impingement except that the effect of shock cells on the mixing zone is dominant. Crafton *et al.*[18] concluded that the impingement angle strongly influences the pressure distribution on the impingement plate, using pressure sensitive paint and particle image velocimetry. Sokolov and Shatalov[19] concentrated on the influence of viscosity in the stagnation region. They showed that size, shape, and number of recirculation zones varies according to the Reynolds number near the impinging plate. Henderson[20] reviewed the investigations on acoustic features of impinging jet and recommended that a better understanding of the flow structure in near wall region will be helpful for unravelling the sound generation mechanisms. Unsteady behaviour of the standoff shock wave was attributed to periodic fluid motion in the recirculation region near the plate. Behind the central portion of the standoff shock wave, the pressure is lower than in the peripheral regions of the jet where the fluid passes through a hanging shock and a reflected shock. This pressure differential leads to a recirculation zone in the central portion of the jet. Carling and Hunt[21] attributed the occurrence of a stagnation bubble to experimental rig design or plate surface finish. A summary of experimental and numerical work[22–43] on impingement noise is summarized in Table I. Even in the absence of impinging tones, the noise generated in an impinging jet could be 10–15 dB more than that in a free jet. Despite this, there is not much work on the noise addition caused due to the wall jet part of the impinging jet. However, there is some work on boundary layer noise, which is discussed in Subsection I B.

B. Turbulent boundary layer noise

In the boundary layer, both the quadrupole and dipole sources arising from the fluctuating Reynolds stress and fluctuating viscous shear stress, respectively, are present. Roughness of surface significantly can enhance boundary-layer noise. Enhancement in the noise for rough surface is mainly due to diffraction. Inhomogeneity produced due to the roughness causes loss of flow energy in the form of friction leading to heat and noise radiation. The diffraction mechanism alters the acoustic source character from quadrupoles to dipoles and thereby causes a significant increase in radiated noise levels.[44,45] Several theoretical studies have been carried out with the aim of predicting some features of the pressure field radiated by a turbulent boundary layer. Lighthill's theory[46] and

TABLE I. List of some major work done during 1950–2010 on aeroacoustics of impinging jets [C: convergent nozzle; CD: convergent-divergent nozzle].

Author(s)	Nozzle	*NPR or n*	*h/d*	Size of plate *D/d* or *L/d* × *W/d*	Area of interest/scope
Marsh[5]	C	1.34[a]	2–20	4[c]	Subsonic impinging noise
Mørch[6]	C	3.83[a]	0.5–2	0.33–1[c]	Shock wave motion and propagation of sound in impinging region
Henderson[7]	CD	1[b]	1–3.5	4[c]	Effect of impinging plate inclination on flow
Gubanova *et al.*[10]	CD	2.85[b]	1,2,3	Large[c]	Phenomenon of stagnation bubble
Donaldson and Snedeker[17]	C	1.25,2.69,6.76[a]	<10	18.40[c]	Detail study of flow structure of impinging jet
Nakatogawa *et al.*[9]	Laval	1[b]	1–24	5 × 5[d]	Shock wave oscillation
Petrie[13]	C	1.2–1.6[a]	1–18	Large[c]	Acoustic power of impinging jets
Semiletenko *et al.*[12]	CD	1.5–4.0[b]	1.1–6.5	Large[c]	Shock wave oscillation depending on nozzle plate spacing
Carling and Hunt[21]	CD	1[b]	0.5	15.7 × 15.7[d]	Exact shape and location of standoff shock
Golubkov *et al.*[22]	CD	1–55[b]	1–12.5	1–8[c]	Flow structure for acoustic radiation from small impinging plate by fluctuating compression shock and fluctuating plate pressure
Gummer and Hunt[23]	CD,C	0, 5, 15[b]	0.5,1,1.5	19.7 × 19.7[d]	Presence of recirculation zone
Ginzburg *et al.*[24]	CD	1.2–36[b]	3–6.5	29.2 × 37.5[d]	Strong and weak instabilities of jet associated with large and small amplitudes oscillation of shock-wave structure
Glaznev *et al.*[25]	CD	6.73[b]	3.5	7.50[c]	Travelling wave in the impingement region
Back and Sarohia[26]	C	1.75–8[b]	1,1.5	7.49 × 7.49[d]	Large oscillations in shock causes large oscillations in plate pressure
Lamont and Hunt[27]	CD	1.2–2[a]	1–15	10[c]	Mean flow properties of impinging jet
Krothapalli[28]	R	2–5.8[a]	10– 30	Large[c]	Origin of choked tones and impinging tones in rectangular impinging jets
Powell[15]	C	2.7–4.74[a]	1.25–6	1, 4[c]	Tone generation from small impinging plate
Norum[16]	RC	1.85–7.3[a]	2.5–20	Large[c]	Simultaneous presence of multiple discrete tones
Iwamoto and Deckker[29]	C	3, 4, 6[a]	0.5–4	16d[c]	Numerical simulation of motion of toroidal vortex in the impinging region
Henderson and Powell[30]	C	2.02–4.74[a]	0.5–10	0.5d–38d[c]	Detailed investigation of tones from large and small plates
Wlezien and Ferraro[31]	C, CD	3,3.5,4[a]	2.8–12.6	9.6 × 9.6[d]	Convergent and convergent-divergent twin nozzles with circular and rectangular exits, acoustic radiation
Messersmith[32]	C,CD	2.5–6[a]	2–6	Large[c]	Application of Powell's feedback model with entrainment velocity of external flow
Levin and Wardwell[33]	C	1.5–6[a]	2–7	Large[c]	Reduction of lift loss in the absence of tones
Krothapalli *et al.*[34]	CD	1–1.35[b]	3–60	96 × 96[d]	Flow structure and acoustic radiation of over- and under-expanded impinging jet
Alvi and Iyer[35]	CD	1.5[b]	1.6–8	39.4 × 39.4[d]	Occurrence of stagnation bubble using plate pressure data
	C	2.5,3.7,5[a]			

TABLE I. (*Continued*.)

Author(s)	Nozzle	*NPR or n*	*h/d*	Size of plate *D/d* or *L/d* × *W/d*	Area of interest/scope
Alvi *et al.*[36]	CD	3.7, 5.0[b]	3.7	Large[c]	Active noise control using micro jets
Krothapalli *et al.*[37]	CD	2.5–5.0[a]	4–60	Large[c]	Passive noise control using control plate
Henderson[20]	C	3.38, 4.74[a]	1–5	12 × 12[d]	Connection between sound production and jet structure of supersonic impinging jets
Travnicek and Tesar[38]	C	Low speed flow	0.5–1	Large[c]	Smoke visualization, annular jet impingement and acoustic excitation of jet
Henderson *et al.*[39]	C	4[a]	1.6–5	21 × 24[d]	Detailed flow visualization using shadowgraph and PIV and acoustic study of impinging jet
Kim and Park[40]	C	1.585–3.0[a]	2.0–4.0	Large[c]	Numerical investigation of impinging jets
Kumar *et al.*[41]	CD	3.7, 5.0[a]	3.7	Large[c]	Particle image velocimetry of active noise control using micro jets
Phalnikar *et al.*[42]	Micro-jet	3.42–7.3[a]	1–8	Large[c]	Flow study of micro-jet impingement on flat plate
Md. Ashraful *et al.*[43]	C	3.0, 4.5[a]	1–3	5[d]	Numerical investigation of supersonic moist air jet impingement

[a]*NPR* (Nozzle Pressure Ratio).
[b]*n* (Underexpansion Ratio).
[c]*D/d* (Ratio of impinging plate diameter to jet exit diameter)
[d]*L/d* × *W/d* (Rectangular impinging plate size). (L and W are length and width of the impinging plate, respectively)

its extensions have then been used extensively in the study of the turbulent boundary layer noise. For instance, Tam[47] used empirical model for the pressure cross-correlation function to calculate the intensity, the directivity and the spectrum of turbulent boundary layer sound field. Howe[48] discussed the impact of unsteady wall shear stress on boundary layer noise and wall pressure fluctuations at subsonic speeds. He developed a theory for noise generation by turbulent boundary layer flow over a sand roughened wall. He also found that over the whole range of frequencies in which roughness noise is significant, viscous effects contributes to 2–3 dB more than predicted by inviscid theory. Howe successfully proved using Lighthill's aeroacoustic theory that noise produced by rough wall is of dipole type. The sliding of turbulent eddies on the wall roughness leads to flow separation and breakdown of shear layers causing vortex shedding responsible for noise. This nonlinear mechanism of flow with rough wall produces more noise than diffraction. Smol'yakov[49] showed the presence of roughness on the surface changes the flow field both quantitatively and qualitatively. First, it amplifies the skin friction in the flow, thus intensifying the turbulent velocity fluctuations within the entire boundary layer thickness causing increase in the quadrupole radiation. Second, the flow gets locally separated due to protuberances of the rough surface, resulting in intense acoustic dipole radiations. Earlier turbulent boundary layers and pipe flows experiments[50] were concentrated on radiated noise, wall-pressure spectra, and their correlations with the mean velocity. Direct noise measurement of turbulent boundary layer noise is difficult since transducers cannot distinguish between sound and pseudo sound (flow perturbations).

Thus, to the knowledge of the authors, there is very little literature available on experimental work on tonal noise and turbulent mixing noise generated from impinging jets and the influence of surface roughness.

C. Motivation

From the literature survey, it is evident that there is immense interest in jet impingement noise from various points of view. It is also seen that impinging jets are noisier than free jet because of

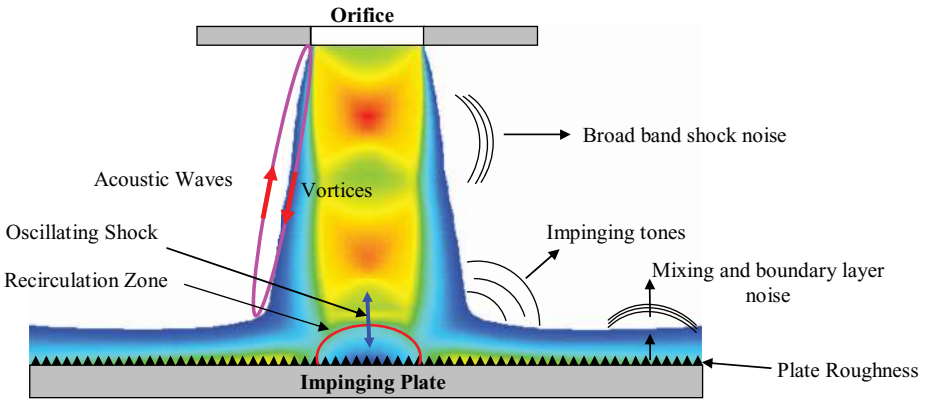

FIG. 1. Flow structure and various acoustic sources present in the impinging jet.

the presence of impinging tones and also due to the presence of the wall-jet. Various noise sources and noise generation mechanisms for impinging jet are schematically represented in Fig. 1. The combination of free jet and wall-jet increases the free shear layer area of the flow. Further, the sound sources are constrained in a smaller region in the impinging jet, compared to a free jet. Thus, the motivation for the present work is to alter the flow structures inside the stagnation/wall-jet regions by varying the plate surface roughness. It is assumed that the plate surface finish would change the wall-jet velocity profile and recirculation zone and hence the overall noise characteristics of the system. Thus, the primary objective of the present work is to investigate the effect of surface roughness of impinging plate on the acoustic radiation. Another novelty of the present work is the fact that orifices are used as jet devices rather than nozzles. Orifices possess negligible boundary layer thickness at the jet exit and enable comparison of various exit geometries. Jothi and Srinivasan[51] reported the effects of initial conditions on pipe jet noise, along with a comparison of pipe jets and orifice jets. Meslem *et al.*[52] compared the flow fields of impinging jets from convergent nozzle and a square-edged orifice having the same exit diameter using particle image velocimetry. They observed that the orifice generates well-defined, energetic Kelvin-Helmholtz structures and larger degree of flow organization with a thin shear layer compared to convergent nozzles. Thin initial boundary layer of the jet leads to steeper velocity profiles and stronger shock-cells in contrast to a thick boundary layer and results in stronger jet screech.[53] Further, orifices are easy to manufacture and install.[54]

The paper outline is as follows. Section II details the experimental setup used in the present study, the uncertainty, and validation of results. In Sec. III, the effect of surface roughness on acoustic radiation with respect to nozzle pressure ratio and nozzle-plate spacing is elaborated by means of blow down experiments, followed by directivity tests and acoustic power calculations for specific nozzle-plate spacing and *NPR* (Nozzle pressure ratio). Section IV discusses the relationship between flow and thermal fields in the impingement region and attempts to relate these results with those obtained earlier. Further, refraction and shielding effects are discussed in this section. A summary of the findings and concluding comments are given in Sec. V.

II. EXPERIMENTAL SETUP AND PROCEDURE

A. Test facility

The test facility comprises the air supply system, jet facility, and acoustic environment. The air is compressed using a two-stage, inner-cooled reciprocating air compressor driven by 150 HP three phase induction motor and stored in the two reservoirs of total capacity of 20 m^3. The compressor and reservoirs are located outside the laboratory and approximately 50 m from the anechoic chamber. The compressor can pressurise the reservoir up to 7.5 bars gauge. Four-inch pipe is used to supply the compressed air from the reservoir to the plenum. Moisture remover and filter are fixed in pipeline to dry and purify the air, respectively. The pressure inside the plenum is regulated using a pressure regulating valve, which is fixed between the supply pipe and plenum. The experiments are carried out

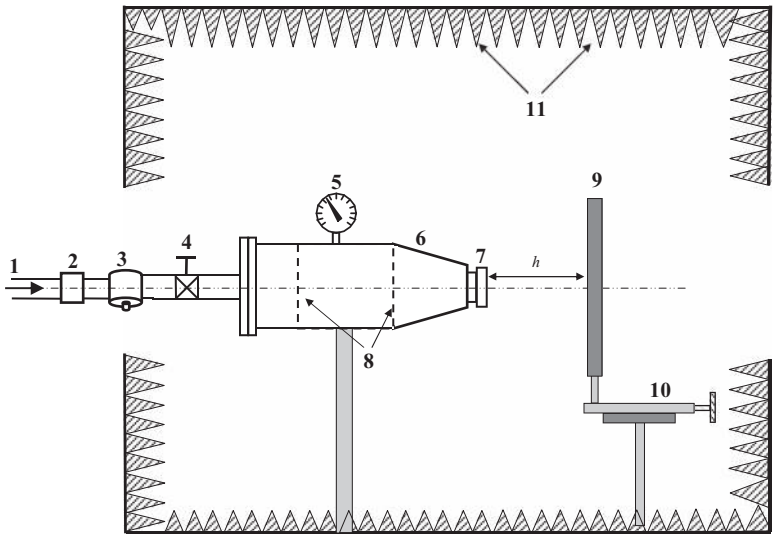

FIG. 2. Schematic view of the impinging jet facility inside the anechoic chamber: 1, air inlet; 2, moisture remover; 3, air filter; 4, pressure regulating valve; 5, pressure gauge; 6, settling chamber; 7, disk holder; 8, wire meshes; 9, impinging plate; 10, linear traverse; and 11, wedges.

in an anechoic chamber of size 2.5 m × 2 m × 2 m (wedge tip-to tip) as shown in Fig. 2. The chamber walls, roof, and door are made of plywood. Square pyramidal polyurethane foam wedges are fixed to all inner surfaces. The floor of the chamber is lined with carpet. The chamber was calibrated using inverse square law to determine the cut-off frequency of 700 Hz. The chamber has two windows to permit entrainment of air and its exit. The cold free-jet test facility consists of a settling chamber fixed inside the anechoic chamber and has the dimensions of 380 mm internal diameter and 700 mm length, connected to a pressure regulating valve by 4-inch pipe at one end and convergent opening at another end to fix the orifice or nozzle. The plenum is converged from 380 mm to 43.5 mm over a length of 100 mm, wherein, the required orifices are mounted using a disk holder. Flow disturbances such as turbulence are mitigated by flow conditioning meshes of progressive fineness at the entry and by providing a convergent section at the exit of the plenum. The structure-borne acoustic disturbances are further lowered by coating the inner wall of the plenum with polyurethane foam. In front of the jet facility, a linear traverse is fixed on which plates of required size can be mounted. The traverse can be used for varying the spacing between jet exit and the plate. To reduce the reflections of acoustic radiation, metallic surfaces such as plenum, disk-holder, traverse, etc. are covered with acoustic foam.

B. Experimental matrix

Orifices of 10 mm diameter (d) drilled on 45 mm diameter plates are used to generate high speed air jet that impinges at the centre of a 300 mm diameter and 15 mm thick aluminium plate. The stand-off distance (h) is varied in the range $1 \leq h/d \leq 10$ in intervals of d. The nozzle pressure ratio is varied from 1.4 to 1.8 in steps of 0.2 (subsonic cases) and 2 to 6, in steps of 1 (underexpanded sonic cases). The plate roughness is varied either by using sand paper or various machining operations. Sand papers are fixed firmly on the metallic surface without disturbing the roughness of sand paper. The roughness values are obtained by using Mahr Pocket Surf III calibrated against Mahr Federal calsurf with certified roughness standard PMD 90101. Roughness of sandpapers and machined surfaces are tested at 17 different locations, three times each. The experimental matrix giving the values of various parameters in the present study are tabulated in Table II and the details of the impingement plate roughness is tabulated in Table III. The various rough surfaces used are denoted as 36 Grit (very rough), 80 Grit, and so on up to 600 Grit (smooth). Table III indicates three different roughness parameters; R_a (arithmetical mean roughness in μm), R_y (distance between the peaks and

TABLE II. Parameters varied during present study.

NPR	1.4, 1.6, 1.8, 2.0, 3.0, 4.0, 5.0, 6.0
h/d	1, 2, 3, 4, 5, 6, 7, 8, 9, 10
Impingement surfaces with sand paper	36 Grit, 80 Grit, 100 Grit, 400 Grit, 600 Grit
Machined impingement surfaces	Aluminium plate with graphite finish aluminium plate with diamond cutting

valleys of the sampled measured normal to surface, in μm), and R_z (ten-point mean roughness in μm). The normalization of these three parameters leads to similar variation, which shows that any one parameter can be used to quantify roughness.

C. Instrumentation

The acoustic data are acquired using $\frac{1}{4}$-inch microphones (B&K 4939 and PCB 377A01) during directivity studies and blow-down experiments. The sensitivity of the microphones used is 4 mV/Pa, and both microphones possess a flat frequency response in the range 4 Hz–70 kHz within $\pm$1 dB. The microphone signal is acquired at a sampling rate of 150 000 samples/s. Aliasing errors in the microphone signals are eliminated by passing the signal through a low-pass analog filter (Krohn-Hite, Model-3364) at 70 kHz. A National Instruments data acquisition board (NI-PCI-6143) is used for acquiring the microphone data. The procedure for acquiring the microphone data for blow-down experiments and directivity studies are explained in the respective sections. A piezo-resistive pressure transducer (Endevco Model 8510C-100) is used for continuous pressure measurement inside the plenum during blow down study. A thermocouple is used to measure the temperature inside the plenum. Flow velocity measurements are made using a 1 mm outer diameter pitot tube connected to MARTEL digital manometer T-140, and a thermal image camera (Fluke Ti32) is used for obtaining the temperature field of the plate.

D. Blow down study

Blow down tests are performed to reveal the noise variation with respect to nozzle pressure ratio. For these tests, microphones are placed at a distance of 10, 30, and 50 jet diameters from the centre of the jet exit at an emission angle of 90°. The reservoir is filled up to 7 bars and then it is drained out through the orifice jet while it impinges on the flat plate. The stagnation pressure is measured continuously using Endevco (model no. 8510C-100) piezo-resistive pressure transducer fixed inside the settling chamber. This test is carried out for impingement plates of various surface roughness values and at different nozzle-plate spacing.

E. Directivity study

This directivity measurement reveals the acoustic intensity distribution in the far field and used to obtain the total acoustic power. An angular traverse is used to study the directivity pattern. Assuming the flow to be axisymmetric, the microphone survey is carried out along a circular path

TABLE III. Various rough surfaces used in experiments.

Test cases	Impingement surface	R_a	R_y	R_z
36 Grit	Sandpaper	125.5	345.5	1215.8
80 Grit	Sandpaper	58.2	181.2	530.5
100 Grit	Sandpaper	33.8	105.3	365.8
400 Grit	Sandpaper	10.6	35.2	110.2
600 Grit	Sandpaper	2.8	12.1	52.1
Fine	Aluminium plate with graphite finish	0.88	6.88	5.8
Smooth	Aluminium plate with diamond cutting	0.063	0.853	0.7

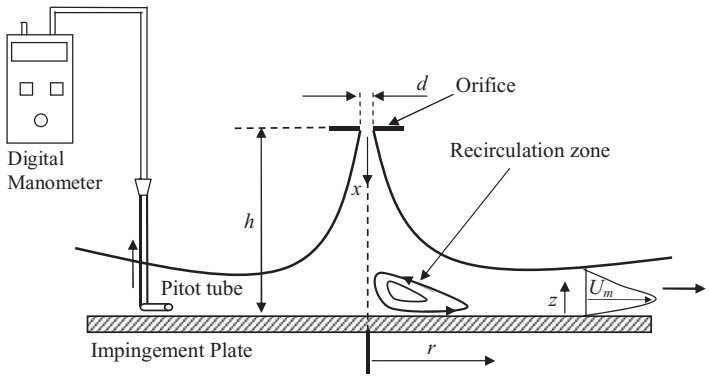

FIG. 3. Schematic of wall jet velocity measurement.

with the jet exit as the centre, and the microphone always facing the centre. The circular path spans from the downstream to the upstream angles, in the range 35°–135° with increment of 5° using angular stepper motor traverse controlled by a LabVIEW program.

F. Velocity and temperature measurement

Wall-jet velocity measurement is carried using a pitot tube of outer diameter of 1 mm, as shown in Fig. 3. The pitot tube is fixed to a linear traverse and moved away from the impinging plate wall to the ambient. Wall-jet velocity profile is obtained at a radius of $r = 10d$ from the impinging plate centre, for plates having different roughness. This study is carried out for the range $2 \leq NPR \leq 6$ in steps of 1. It is very difficult to obtain the pressure field on the plate since pressure taps would alter the roughness of the plate. Yaga *et al.*[55] observed from their experiments on rectangular impinging jet that the pressure and temperature contours are qualitatively similar in the stagnation region. Therefore, instead of measuring the pressure field, the thermal field is captured using the thermal imaging camera by focusing on the stagnation region. Settling time of 3 min was found to be adequate for attainment of thermal equilibrium in the stagnation region for a particular flow/geometry setting. Since thermal images are sensitive to distance and the emissivity of the material under observation, a constant camera distance is maintained, and an emissivity value of 0.95 is used for the black coloured sand paper. The captured thermal pictures are processed using SmartView software. Further data processing and presentation are performed using MATLAB 8.0.

G. Uncertainty analysis and validation of results

The microphones are calibrated using a B&K pistonphone type 4228 calibrator (single point calibration at 250 Hz and 124 dB). The piezo-resistive transducer employed for pressure measurement during blow down has an uncertainty of ±0.2% of full scale. The anechoic room environment (28 °C and relative humidity, 80%) is nearly constant with a maximum temperature variation of ±1 °C and ±2% variation in relative humidity for each trial of experiment. The sound pressure level reported here is relative to the reference pressure of 20 μPa. The frequency resolution based on the FFT (Fast Fourier Transform) size is 37 Hz over the range of frequency from 700 Hz to 70 kHz. The overall measurement error in acoustic data (*OASPL* – OverAll Sound Pressure Level (dB reference 20 μPa)) including repeatability errors is within ±1.0 dB. The microphone positioning error is within ±1.0 mm and microphone angle within ±1°. The error in the nozzle-plate spacing is ±0.2 mm and the uncertainty in pitot velocity measurement is 2%. Acoustic data and velocity data are validated against available literature, as detailed below.

Acoustic data are validated by comparing the experimental screech frequency with the choked jet screech frequency formula[56] for 3 orifices of 8, 10, and 12 mm diameters. Figure 4 shows that the free jet from 8 mm orifice exhibits the same trend observed by Gao and Li.[56] However, 10 and 12 mm orifices show only helical modes. Further blow down of free jet data is used to validate the acoustic strength. Figure 5 shows *OASPL* (with and without tones) superimposed on the spectral

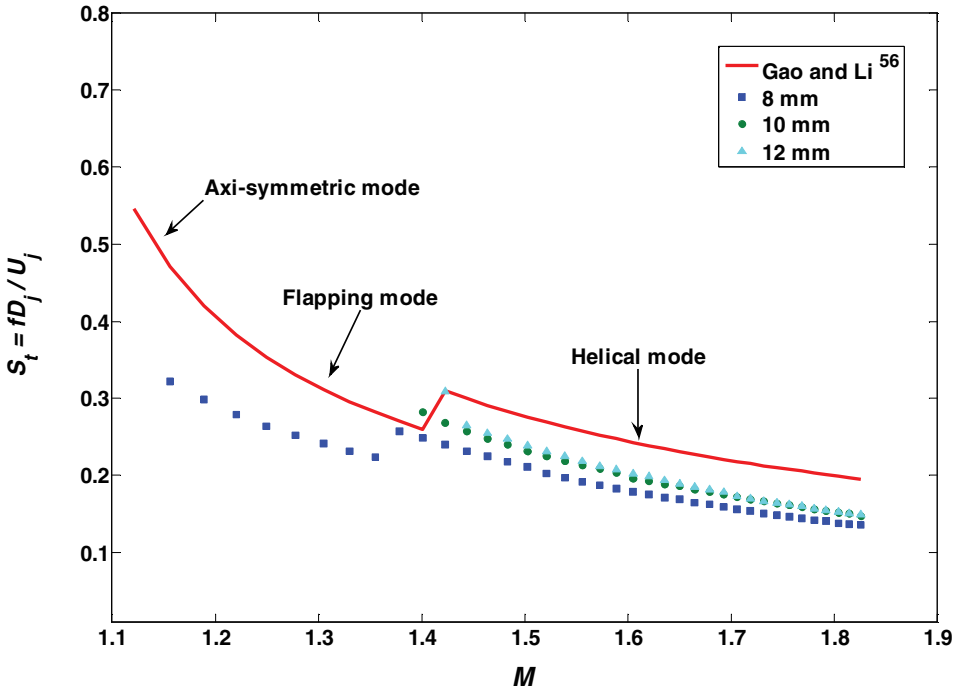

FIG. 4. Screech frequency validation of free jet with screech formula modified by Gao and Li.[56]

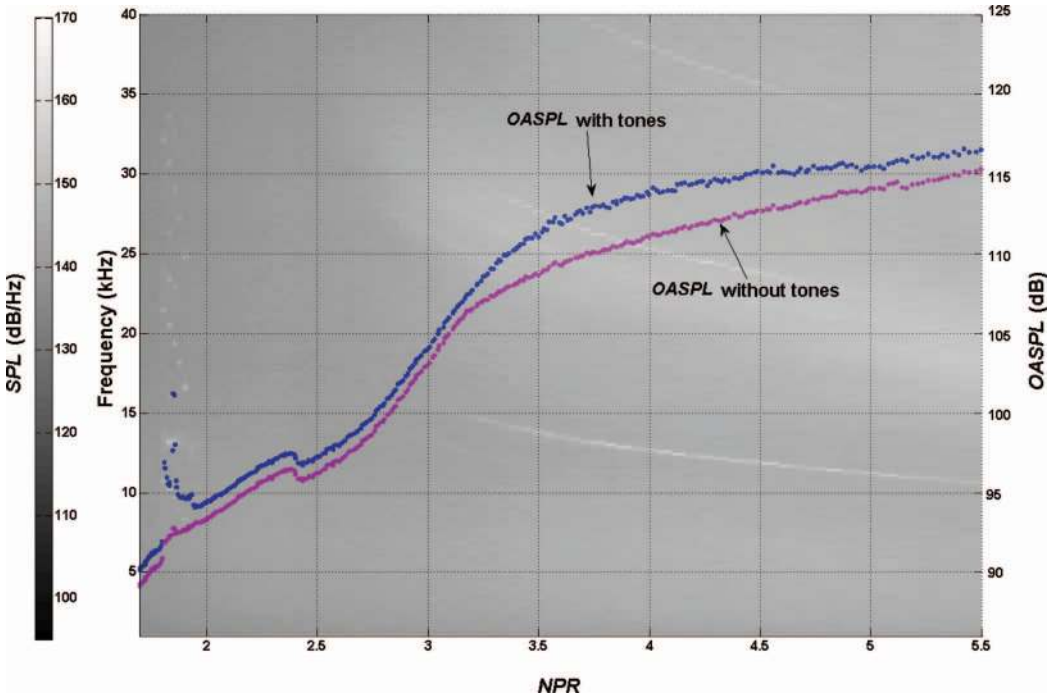

FIG. 5. Dominant tones (screech) and turbulent noise variation for free jet with respect to *NPR* and *OASPL* variation with and without tones.

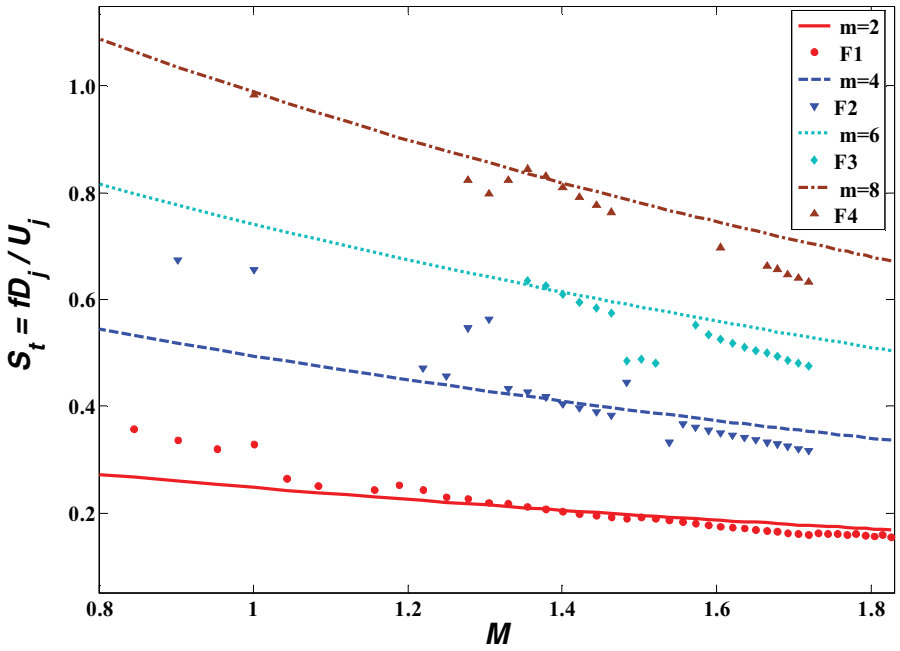

FIG. 6. Frequency validation of impinging jet using staging frequency formula.

color map. The *OASPL* curve follows well known U_j^8 (for subsonic region) and U_j^3 (for supersonic region) variation of acoustic power for free jets. For validation of impinging jet acoustic data, staging frequency formula is used.[34] Figure 6 shows that the fundamental impinging frequency coincides with the formula, although the harmonics show a minor deviation. It is difficult to validate the noise level as it depends on several factors: initial flow conditions, geometry, upstream conditions, environmental conditions, and so on. However, the trends of *OASPL* in subsonic impinging jet are

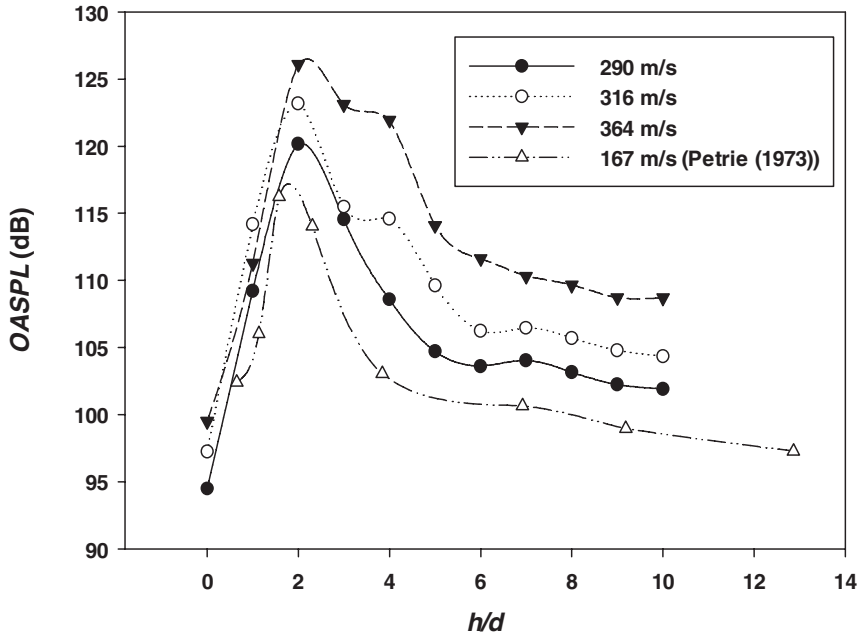

FIG. 7. Effect of nozzle-plate spacing on *OASPL*.

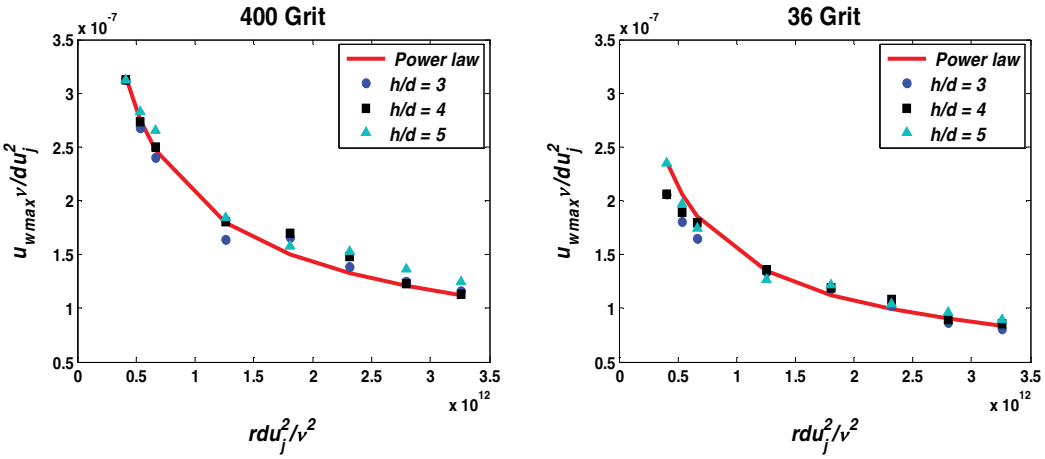

FIG. 8. Maximum velocity of wall jet velocity validation using Power law expression and independent of nozzle-plate spacing.

comparable with the results of Petrie.[13] It is found that the *OASPL* increases with *h/d* up to $h/d = 2$ and then decreases (Fig. 7).

Validation of wall jet velocity profile requires the details of flow such as nozzle exit velocity profile and impinging plate characteristics (surface roughness and shape). However, for unconfined turbulent wall jets, the maximum velocity can be expressed in a power-law form.[57] It is interesting to note that these expressions are independent of nozzle-plate spacing, and verified from experimental data for smooth and rough impinging surfaces at $r/d = 10$. Figure 8 shows the experimental and empirical results with values of $k_1 = 0.2$ and $k_2 = -0.5$ for 400 Grit and $k_1 = 0.15$ and $k_2 = -0.5$ for 36 Grit.

III. RESULTS AND DISCUSSION

The time domain acoustic signals acquired by the microphones are analyzed using MATLAB 8.0 to obtain the overall sound pressure level, turbulent mixing noise, tonal frequency, and amplitude. As mentioned earlier, the time series data of 150 000 points acquired for a period of one second, is analyzed using 4096 FFT points, yielding a frequency resolution of 37 Hz. The acoustical results are presented in the following order: First, *OASPL* results for various rough surfaces placed at different stand-off distances obtained during blow down are compared. Second, dominant tones and their harmonics are compared for various surfaces at $h/d = 4.0$ and variation of spectra with respect to *NPR* for 36 Grit surface at $h/d = 5.0$ is demonstrated. Later, *OASPL* is recalculated by eliminating the tones from the spectra to study the effect of various parameters on the mixing noise. Finally, the sound pressure directivity is measured for a few values of *NPR* and *h/d* to estimate the acoustic power for these cases.

A. Overall sound pressure level (*OASPL*)

In order to effectively investigate the variation of acoustic characteristics with stagnation pressure, blow down studies are carried out using plates having different surface roughness placed at various spacing distances from the orifice ($1 \le h/d \le 10$ with an interval of d). The same experiments are repeated for free jets (without impingement plate). It is observed that the noise generated by impinging jet is comparable to free jet at $8d$ for $NPR \le 3$ and $10d$ for $4 \le NPR \le 6$. The presence of the plate is most dominant within $6d$. Experiments carried out for $h/d = 1$ and 2, are not presented mainly because of the erosion of sand paper due to high suction force (60% of the jet thrust, for instance, in Krothapalli *et al.*[36,37]). The effect of roughness at $6d$ standoff distance is insignificant. Therefore, stand-off distances of $h/d = 3$, 4, and 5 are examined closely. As shown in Fig. 9,

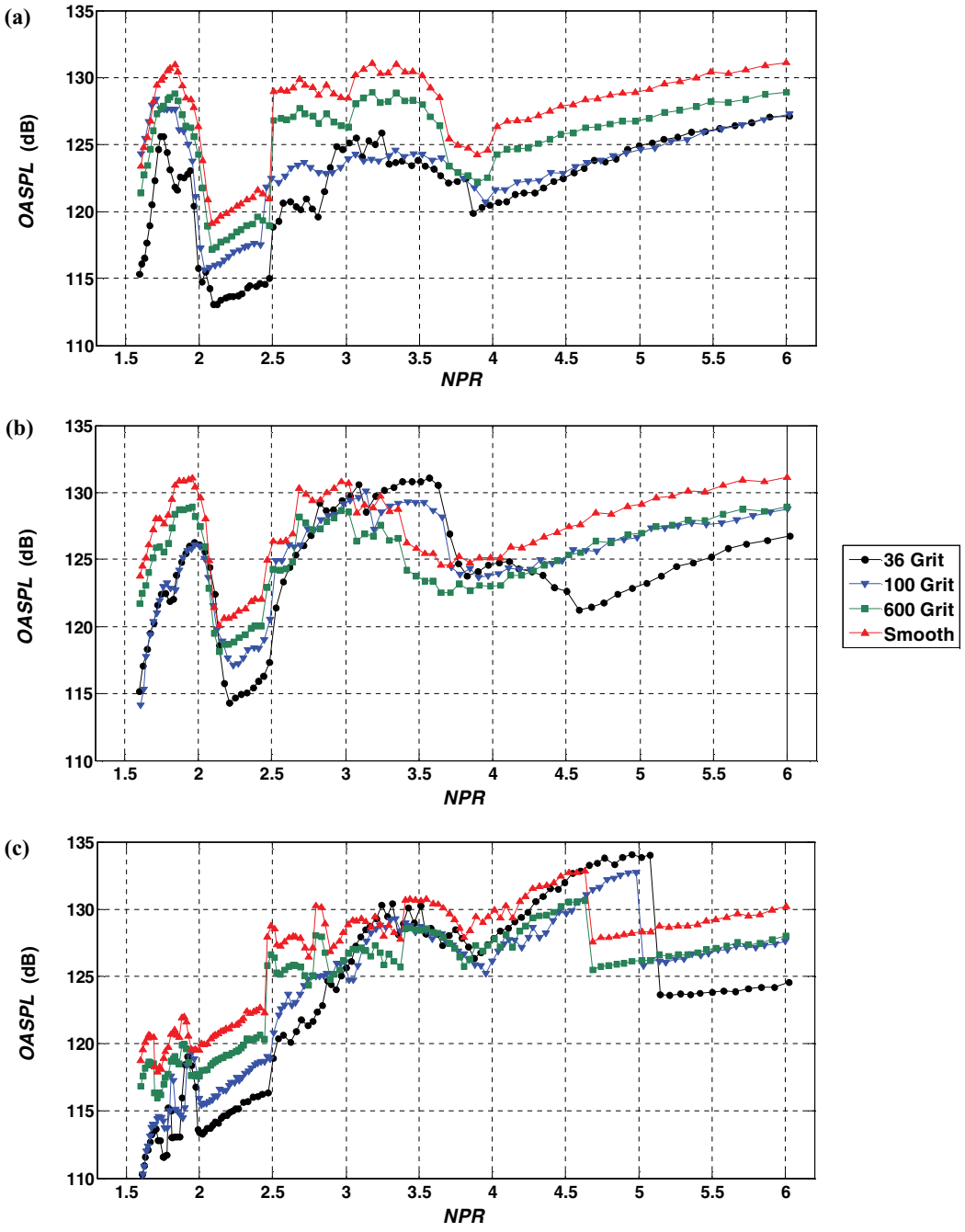

FIG. 9. Variation of *OASPL* with *NPR* obtained by performing blow down test for different plate roughness at (a) $h/d = 3.0$, (b) $h/d = 4.0$, and (c) $h/d = 5.0$.

OASPL increases as *NPR* increases in the subsonic region irrespective of stand-off distance. There is a prominent transonic (*NPR* around 1.9) effect for all impinging surfaces wherein the *OASPL* values shoot up and decrease in the initial supersonic region ($NPR \sim 2$). Then on, the *OASPL* shows increasing trend with increasing reservoir pressure up to $NPR = 2.5$. At $NPR \sim 2.5$, a sharp increase is observed for $h/d = 3$, 4, and 5 for all surface roughness values. It can be seen from Fig. 9(a) that at $h/d = 3$, *OASPL* decreases at lower values of *NPR* in the case of smooth impinging surfaces ($NPR = 3.6$) compared to rough impinging surfaces ($NPR = 3.8$). Similarly Figs. 9(b) and 9(c) show early *OASPL* decline for smooth surfaces than rough surfaces. For $h/d = 4$ the *OASPL* reduction

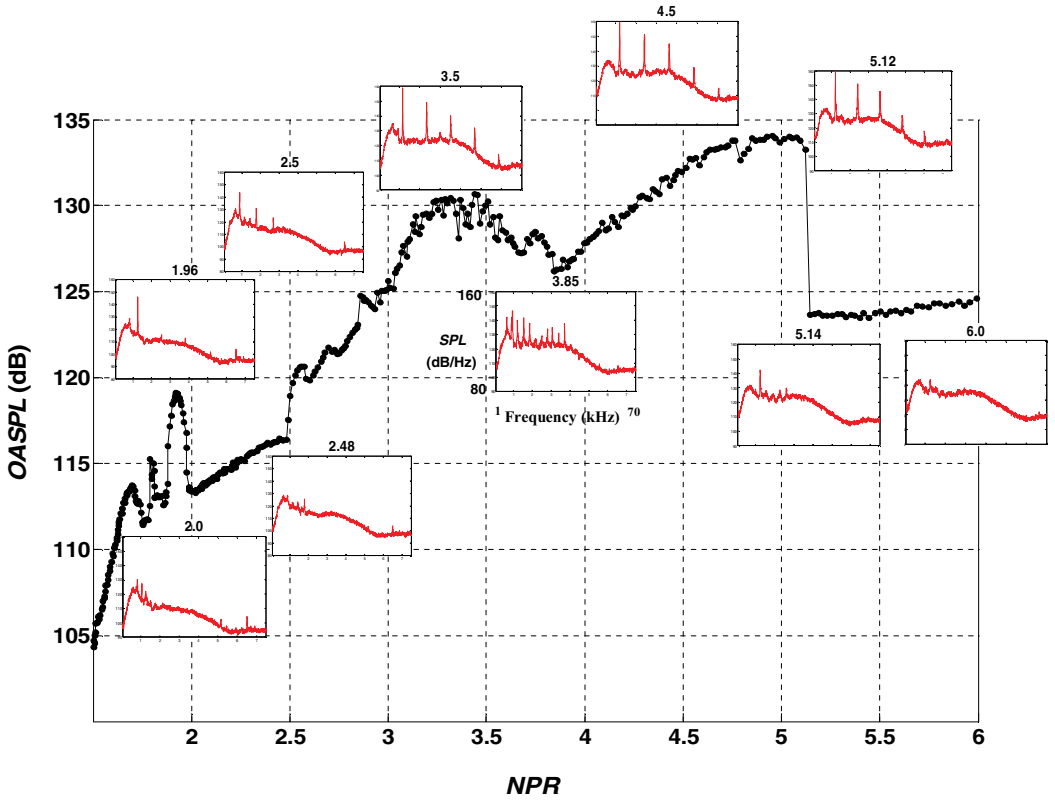

FIG. 10. Variation of *OASPL* with respect to *NPR* for 36 Grit roughness at $h/d = 5.0$ with some spectra.

is seen approximately at $NPR = 3.4$ for smooth surfaces where as for rough surfaces it occurs at $NPR = 3.75$. For $h/d = 5$ the *OASPL* fall is seen approximately at $NPR = 4.7$ for smooth surfaces whereas for 100 and 36 Grit (rough) surface it occurs at $NPR = 5.0$ and 5.2, respectively. For $NPR > 2.2$, except the region with impinging tones and its harmonics observed in the *NPR*-*OASPL* curve, the roughness of plate causes a decrease in *OASPL*. This exception may be due to the dominance of tones caused by asymmetric mode of jet disturbance at moderate pressure ratios,[15] which are independent of surface roughness of the impinging plate. However, it is observed that roughness of plate widens the staging region. The spectral analysis (discussed in Sec. III B) shows the presence of discrete tones whenever there is jump in *OASPL*. It is clearly observed that rough surfaces produce less noise than smooth surfaces in the regions other than staging, wherein stagnation region plays a dominant role.

B. Spectral analysis

In order to understand the cause of the *OASPL* peaks observed earlier, spectral analysis is conducted on the signals. The *OASPL* vs *NPR* plot is shown in Fig. 10 with spectra at various *NPR*s shown as insets. A *h/d* value of 5.0 is chosen for this presentation since the spectra are predominantly tonal. This plot reveals that the sudden rise and fall of *OASPL* vs *NPR* curve depends on appearance of pure tones. Wherever a sudden peak in *OASPL* is observed, the spectra possess pure tone and its harmonics. This trend is observed in all cases discussed in Sec. III A. Further, the *OASPL* data for impinging noise for $h/d = 4.0$ are superimposed on the frequency-*NPR* plane in Fig. 11. The color-bar denotes the power spectral density of the coloured contours in the Frequency-*NPR* plane, and the right hand side ordinate represents the *OASPL*. It is observed from the figure that the most significant variation is within 1–30 *kHz* for $NPR = 1.8-5.5$. It is also illuminating to note that wherever the *OASPL* is higher, tones of higher amplitudes are present. For rough surfaces such as

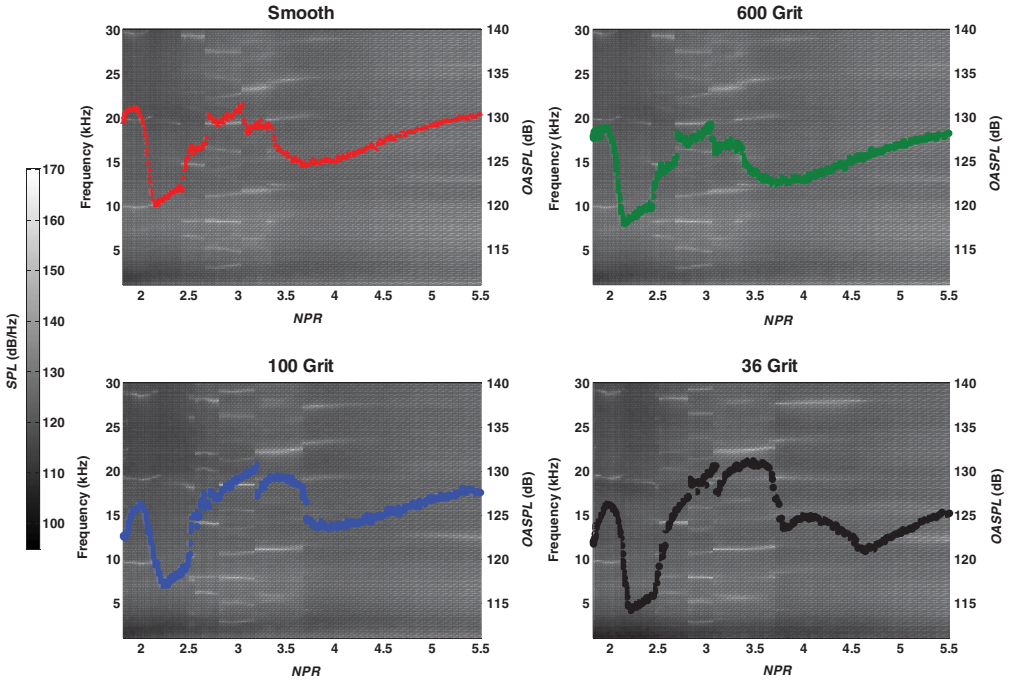

FIG. 11. Dominant tone and turbulent noise variation for various impinging surfaces with respect to *NPR* at $h/d = 4.0$.

36 and 100 Grits, frequency and amplitude of tones (and their harmonics) are comparable. Similarly smooth surfaces (600 Grit sand paper surface and diamond-cut finished surface) are nearly identical in terms of tonal frequency and amplitude. In case of rough surfaces the harmonics are dominant compare to smooth. Also evident in Fig. 11 is how the *OASPL* varies for different surfaces with respect to *NPR*. For smooth and 600 Grit surfaces, the amplitude is higher at almost all frequencies compared to 100 and 36 Grit impinging surfaces. For smooth and 600 Grit plates the dominant tones and their harmonics are visible in the range $2.5 \leq NPR \leq 3.5$. In the case of 100 Grit and 36 Grit plates, the dominant tones start appearing at around $NPR = 2.5$ but continue until $NPR = 3.7$ and 3.8, respectively. These tonal amplitudes are 15−25 dB more than broadband noise for all impinging surfaces.

C. Turbulent noise

It can be concluded from the spectral analysis that surface roughness alters the frequency and amplitude of pure tone or its harmonics. In order to delineate the turbulent mixing noise from the peak-dominated spectra, the discrete tones in the spectra are removed by clipping the tones as shown in Fig. 12. The remaining tone-less spectra are shown in Fig. 13. Turbulent noise curves for all roughened surface show the same trend as the free jet as shown in Fig. 5, with some shift. Further, these figures illustrate that roughness of impinging plate reduces turbulent noise for all pressure ratios. These results are contradictory to the low velocity boundary layer noise reported by Howe[45] and Smol'yakov.[49] However, their experiments concerned the boundary layer noise and they used 50–80 grit size sandpaper.

D. Tonal noise

From the rich literature on impinging jets, it is evident that feedback loop mechanism is responsible for the generation of impinging tones. It is seen that for rough surfaces, the tonal frequencies are slightly less compared to smooth surfaces. The occurrence of such distinct tones for given *h/d* widens the region for rough impinging surfaces on *NPR* vs *OASPL* plot as shown in

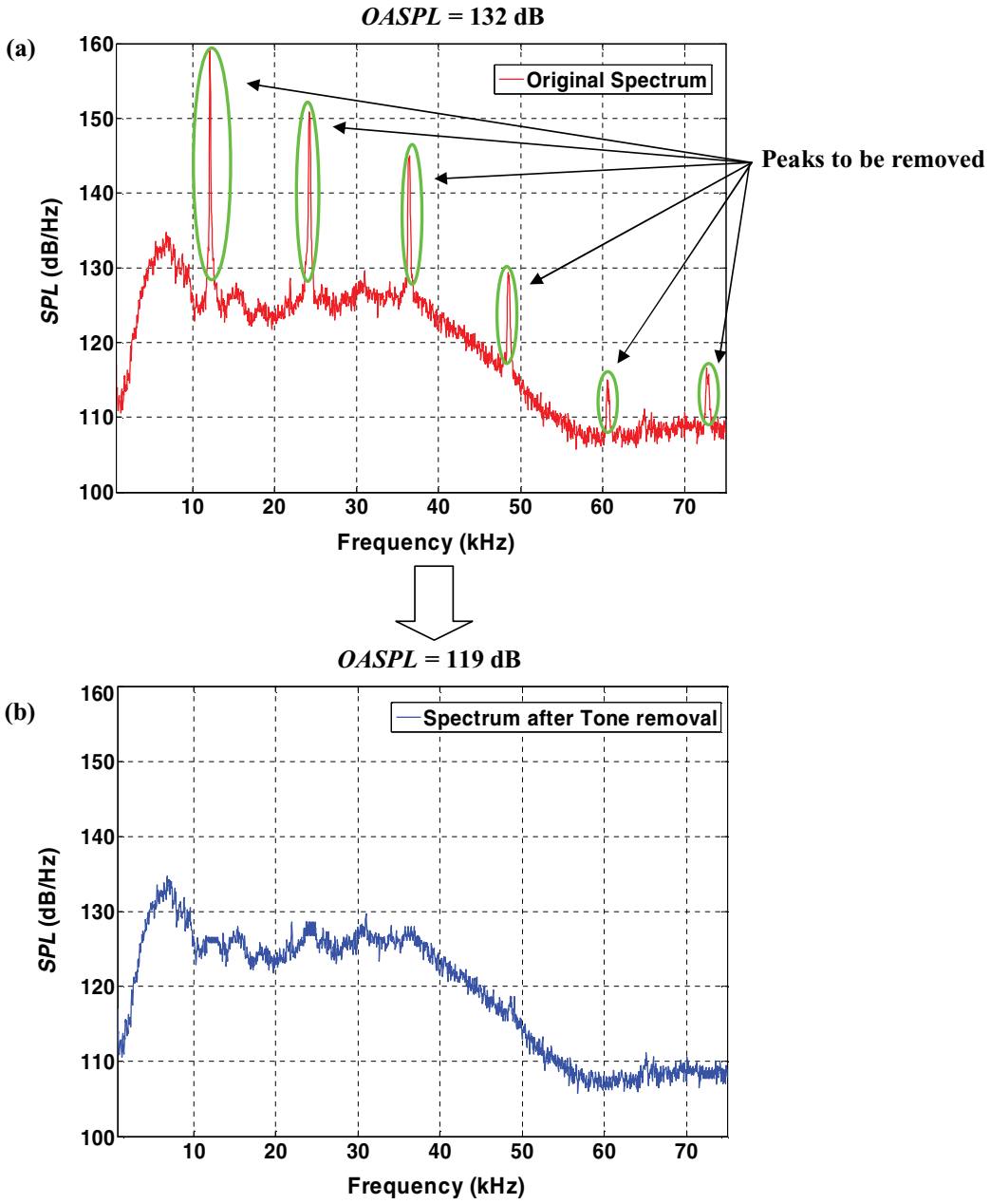

FIG. 12. (a) Original and (b) tonal removed spectrum for jet impinging on 36 Grit surface at $NPR = 4.5$ at $h/d = 5.0$.

Fig. 9. The ups and downs of *OASPL* is attributed to the transition of impinging tones from one mode to another. This mode switching is confirmed using 3 microphone techniques for one of the cases observed at $NPR = 3.85$ and $h/d = 5$ for jet impinging on the 36 grit surface. Figure 10 indicates that sudden increase in *OASPL* at $NPR = 2.5$ is due to the presence of impinging tone (11 760 Hz frequency) whose amplitude and number of harmonics increase with *NPR*. Further it is seen that the spectra at $NPR = 3.5$ contains four harmonics of high amplitudes. After $NPR = 3.5$ *OASPL* starts decreasing slowly up to $NPR = 3.85$ and then slowly increases up to $NPR = 5.1$. To investigate this decrease and increase of *OASPL* even in the presence of impinging tones, various spectra available in this region are studied. It is seen that two non-harmonically related frequencies (11 760 Hz and 12 100 Hz, with ± 37 Hz uncertainty) dominate the spectra in the range $3.55 \leq NPR \leq 4.0$. Therein, the amplitude corresponding to 11 760 Hz component (and its

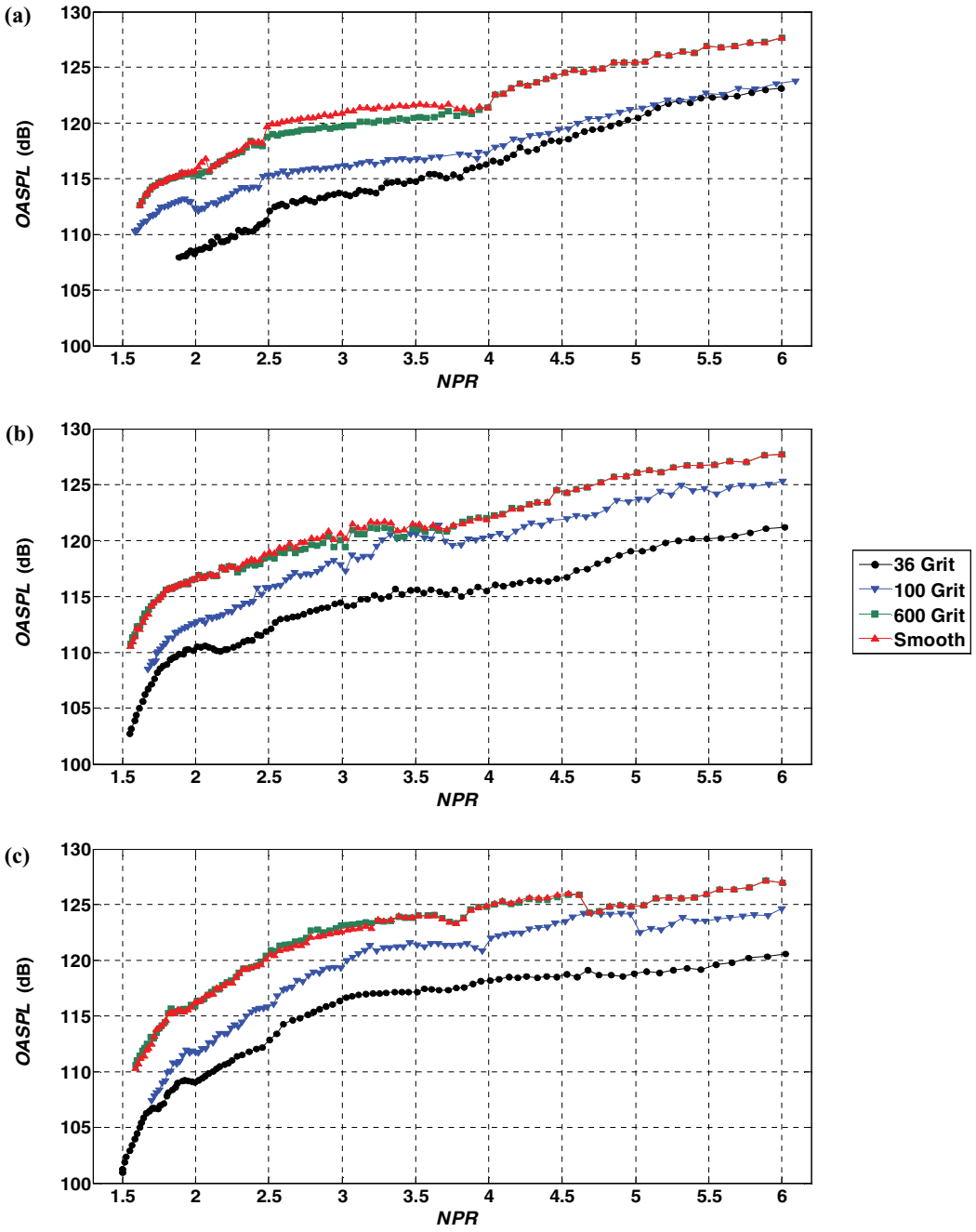

FIG. 13. Variation of *OASPL* with *NPR* after elimination of tones for different plate roughness at (a) $h/d = 3.0$, (b) $h/d = 4.0$, and (c) $h/d = 5.0$.

harmonics) slowly decreases, while the amplitude corresponding to the 12 100 Hz component (and its harmonics) increases. The transition from 11 760 Hz to 12 100 Hz is complete at around $NPR = 4.5$, where only the 12 100 Hz component dominates. The three-microphone study is conducted by placing the 3 microphones on a circle of $5d$ radius at the nozzle exit plane, such that the microphone positions are at an angle 90° to each other, as shown in Fig. 14. The phase difference between the microphones is found using cross-correlation. Figure 14 clearly shows there is a mode switch at $NPR = 3.85$. For further understanding of the results, directivity study is carried out and presented in Sec. III E.

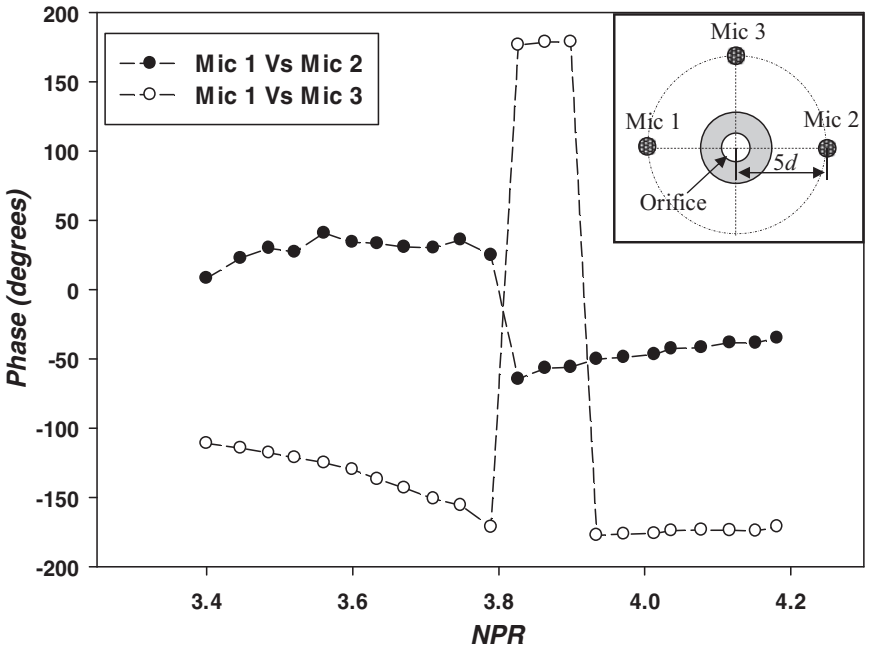

FIG. 14. Variation of phase difference with *NPR* for 36 grit impinging plate at $h/d = 5.0$.

E. Directivity study and acoustic power

Directivity study is carried out for finding the sound pressure level distribution around the impinging jet setup and to calculate the total acoustic power radiated. Directivity study is carried out for impinging jet with stand-off distance $h/d = 3$, 4, and 5, for emission angles in the range $35^\circ \leq \theta \leq 135^\circ$ at $R_j = 30d$ using an angular traverse. For all the pressure ratios and stand-off distances, the overall pressure level increases as the microphone moves towards the impinging plate due to the convection of sources. Then, the *OASPL* suddenly decreases due to the presence of the wall-jet. This decrease observed in impinging jet is similar to the well known refraction effect observed in free jets.[58] Further decrease in *OASPL* is due to the blocking of noise by the plate or shielding of sound by the wall-jet. Figure 15 shows the directivity plots for various rough surfaces for a few combinations of *NPR* and *h/d*. It is observed in Figs. 15(a) and 15(c) that in the forward angles ($90^\circ \leq \theta \leq 135^\circ$), roughness has a monotonic effect with respect to *OASPL* for cases that are not tone-dominant. However, if the spectra are dominant with tones, the surface roughness effect is not clearly visible, as in Fig. 15(b). From Fig. 15, it is also seen that in the aft angles ($35^\circ \leq \theta < 90^\circ$), i.e., on the rear side of the plate, roughness effects are not predominant. This is due to the effects of wall-jet shielding and sound shielding by the plate. In angles close to 90°, effects of pseudo-sound are observed due to the microphone positioned against the wall-jet flow direction. Since the effect of surface roughness is not brought out clearly in tone-dominated cases such as Fig. 15(b), it is worthwhile analysing the tone-less *OASPL* for these cases. The results of tone-less *OASPL* variations are shown in Fig. 16. It is observed that *OASPL* monotonically decreases with increasing surface roughness in regions between the jet and the plate, apart from the wall-jet region.

Acoustic power (*AP*) radiated is calculated using the integral in Eq. (1)

$$AP = 2\pi R_j^2 \int_{\theta_1}^{\theta_2} I \sin\theta d\theta, \tag{1}$$

where I is the acoustic intensity, R_j is the radius at which directivity is measured, and θ is the measurement angle with respect to jet axis. Figure 17 shows the acoustic power for various rough surfaces and *NPR*s at *h/d* value of 3. The figure indicates that surface roughness, in general, attenuates

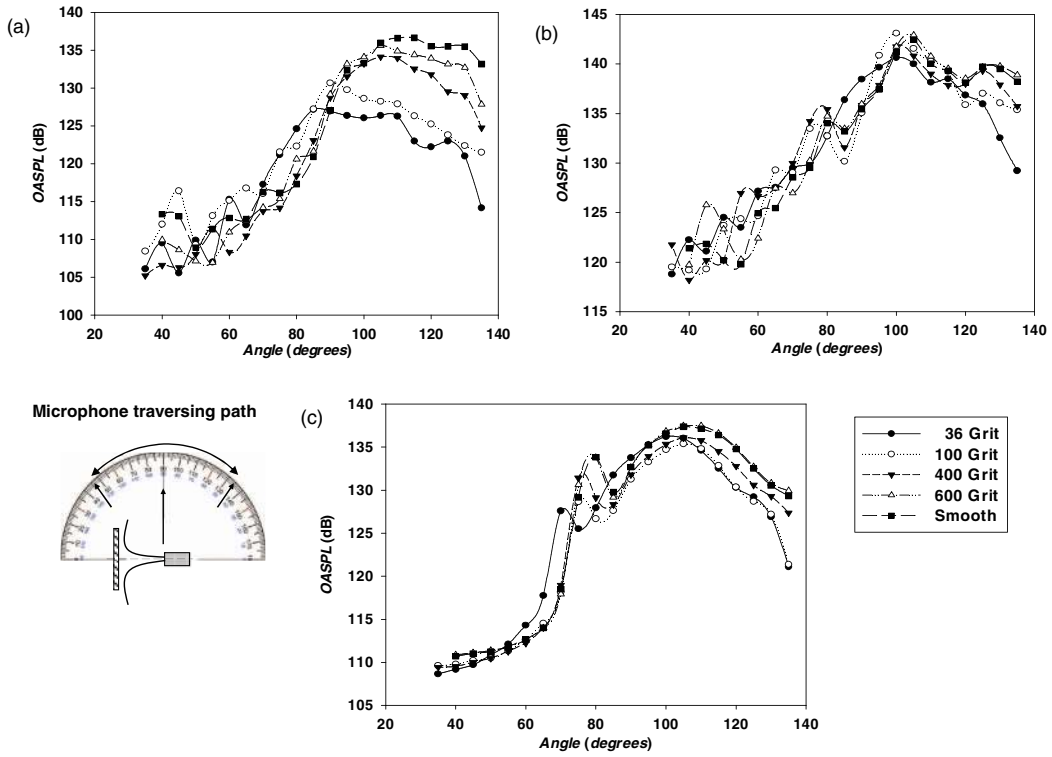

FIG. 15. *OASPL* directivity pattern for different roughness with (a) $h/d = 3.0$, $NPR = 2.0$; (b) $h/d = 5.0$, $NPR = 4.0$; and (c) $h/d = 5.0$, $NPR = 5.0$.

noise, leading to lower values of acoustic power. A monotonic variation is not observed due to the presence of tones in some cases. In underexpanded cases, for a given surface roughness, acoustic power does not vary monotonically with *NPR*. This is again due to the presence of tones at certain *NPR*s. Therefore, in order to bring out the effect of surface roughness, toneless acoustic power is calculated and presented in Fig. 18. This metric gives the acoustic energy emitted from the turbulent mixing process in the shear layer of the impinging jet. Figure 18 shows a monotonic decrease in acoustic power with respect to roughness. The amount of decrease in acoustic power is more significant for high speed impinging jets.

Next, an attempt is made to derive a theoretical estimate of directivity pattern from the results available in the literature and compare them with the present experimental results. A simplified basic broadband directional pattern radiated from unit volume at y, for free jet can be expressed as[58]

$$AP(y,\theta) = C^{-5}\left[A + \frac{B}{2}\left(\cos^4\theta + \cos^2\theta\right)\right], \tag{2}$$

where A is the self noise due to the turbulence velocity and independent of mean flow and B is the shear noise, generated due to cross-coupling of mean flow and instantaneous fluctuation C is

$$C = \sqrt{\left[(1 - M_c\cos\theta)^2 + \omega_f^2 L^2/\pi c^2\right]} = \sqrt{\left[(1 - M_c\cos\theta)^2 + \alpha^2 M c^2\right]}. \tag{3}$$

In the above equation, M_c is the convective Mach number, c is the ambient speed of sound, ω_f is the characteristic frequency, L is the turbulence length scale, and α is a non-dimensional parameter. The suggested value of α is around 0.55, the details of which can be found in Ribner.[58] Directivity of impinging jet can be found by superimposing the directivities of two appropriately oriented jets. The schematic representation of this method is shown in Fig. 19. Figure 19(a) shows the transformation of jet noise due to superposition of various effects such as shear noise, convection and refraction. Similar superposition effects in impinging jet configuration is shown in Fig. 19(b), in which, the

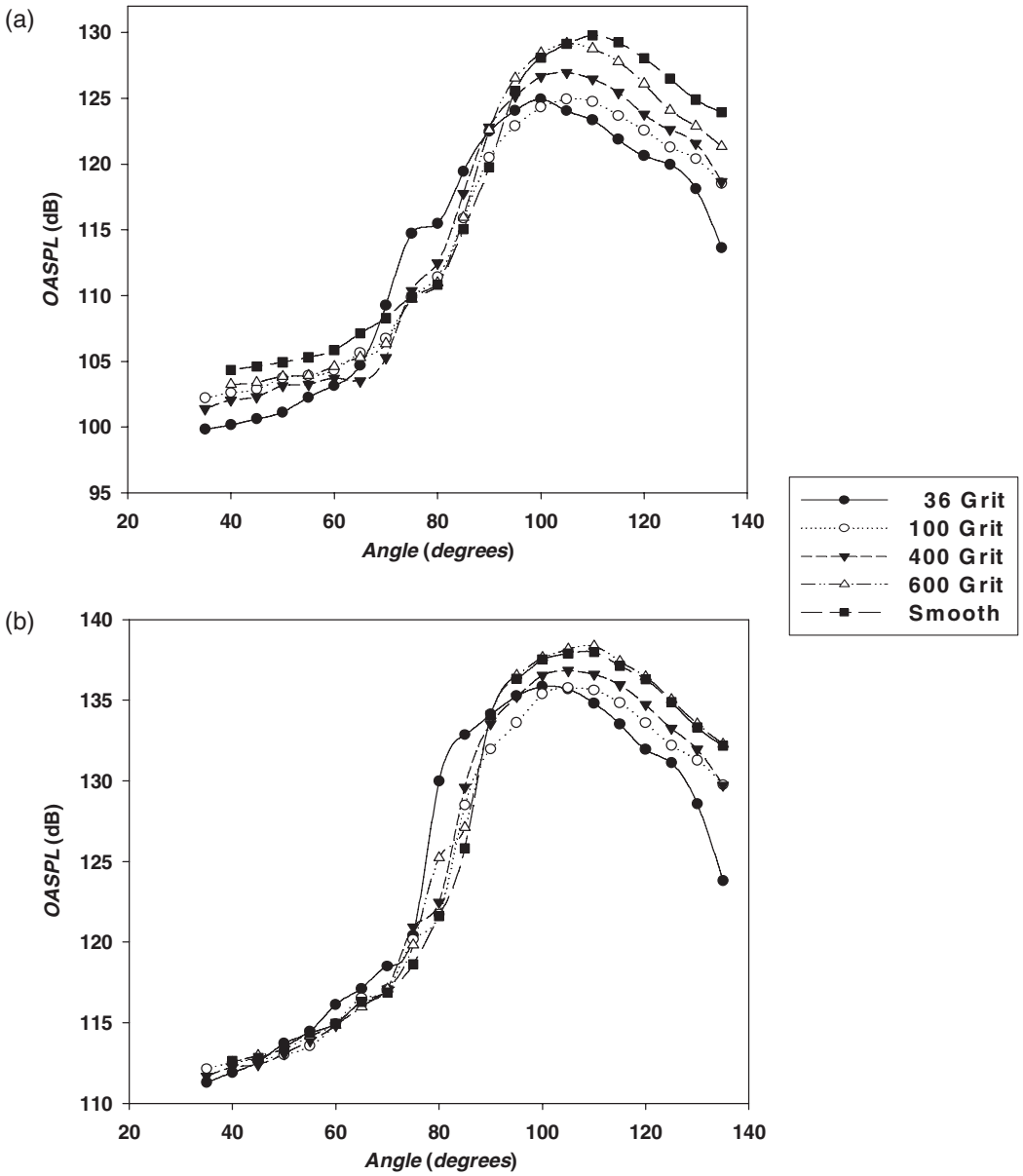

FIG. 16. *OASPL* directivity pattern after elimination of tones for different roughness with (a) $h/d = 3.0$, $NPR = 2.0$ and (b) $h/d = 5.0$, $NPR = 4.0$.

impinging jet directivity is constructed from the directivity patterns of free jet and wall-jet. The shielding effects caused by the impinging plate are not considered here. Finally, it may be concluded that the directivity of impinging jet can be divided in four regions as shown in Fig. 20. The region behind the impinging plate, where the sound pressure level increases with angle and the region is influenced by the sound attenuation characteristics of the plate. The next region falls directly against the wall-jet, and influenced by the fluid flow, and is therefore, pseudo-sound, depending on the measurement radius. As the angle increases, the next region is dominated by the effect of refraction through the wall jet shear layer. The last region, in which the pressure level deceases with angle, is free from all effects such as refraction, sound attenuation characteristics of the plate, wind velocity and so on.

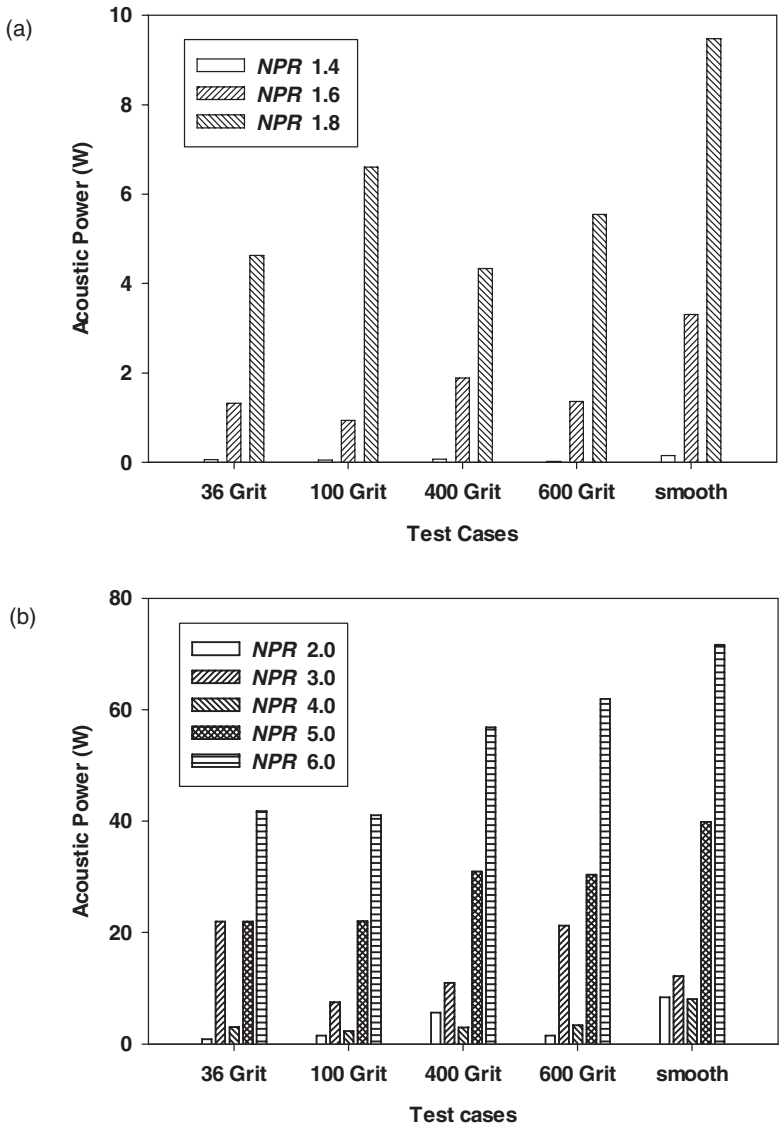

FIG. 17. Acoustic power for different surface roughness at $h/d = 3.0$ for (a) subsonic cases and (b) underexpanded cases.

IV. ROLE OF FLOW FEATURES ON THE NOISE

The purpose of this section is to explain the results obtained in Sec. III. This section is divided into three subsections. First, temperature measurement in the stagnation region attempts to explain the impinging tonal characteristics. Second, wall-jet velocity measurement shows the influence of roughness on the mean velocity profile of wall-jet and third a separate experiment explains the effect of noise source shielding by the wall-jet shear layer.

A. Temperature field in the stagnation region

To understand the physics behind the reduction in *OASPL* and appearance of tones, a detailed flow description is warranted. The surface roughness of the plate can alter stagnation region, wall-jet and not the free-jet zone. It is very difficult to measure the pressure distribution on the plate, as pressure tappings may affect the roughness characteristics. Therefore, temperature distribution by non-intrusive means is a good alternative to infer the flow features without disturbing the flow and

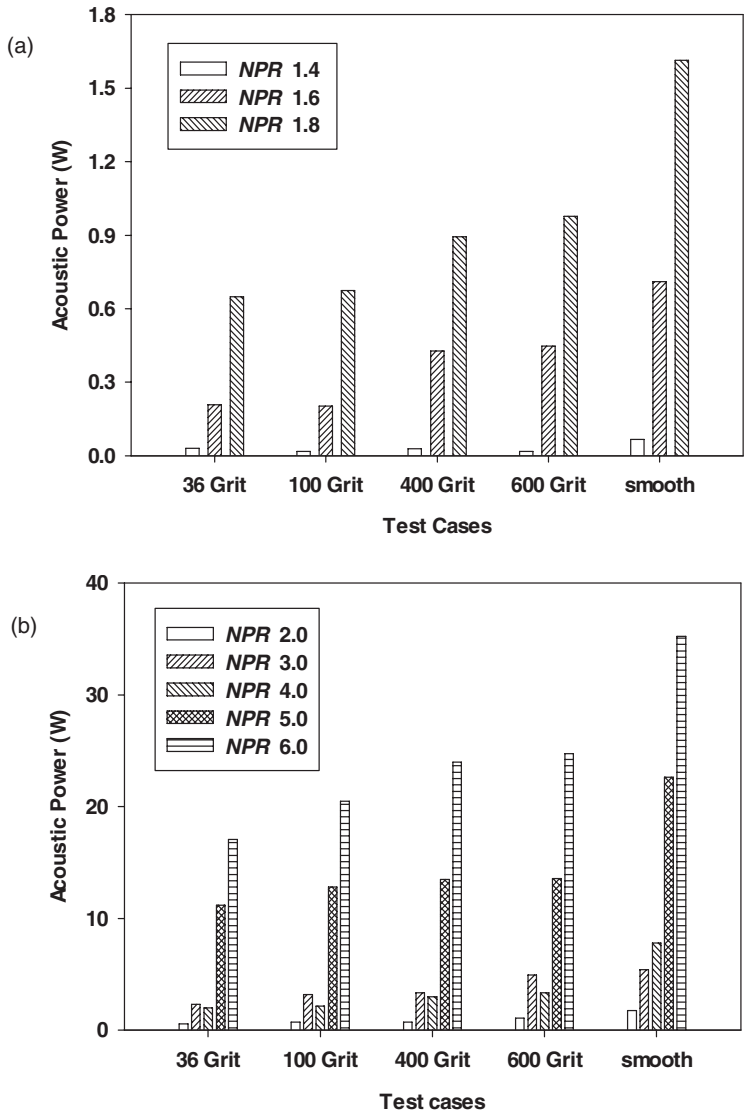

FIG. 18. Acoustic power after eliminating tonal power for different surface roughness at $h/d = 3.0$ for (a) subsonic cases and (b) underexpanded cases.

roughness of the plate. An infra-red camera is employed for the purpose. Yaga *et al.*,[55] while working on flow characteristics of underexpanded rectangular impinging jets, showed that pressure contours and temperature contours are almost identical.

Temperature images of the plate are captured for all the test cases and for different *NPR* from 1.4 to 6.0 with interval 0.2. Figure 21 shows the same variation of *OASPL* with *NPR* as in Fig. 10, except that in Fig. 21 temperature distribution images are included as insets. From these images, and from Fig. 10, it is clear that whenever the tone is present, the temperature at the stagnation region is high. Variation of recirculation zone near the impinging zone leads to different temperature contours as shown in Fig. 21.

Figure 22 indicates that roughness of the plate changes the shape and size of recirculation zone. These flow features can in turn modify the frequency and SPL (Sound Pressure Level in dB reference 20 μPa) or amplitude of discrete tones for $h/d = 3.0$ and $NPR = 3.0$ as shown in Fig. 23(a). Figure 23(a) also indicates that the tonal frequency and amplitude do not vary monotonically with roughness, thus masking the effect of surface roughness. However, in the absence of these

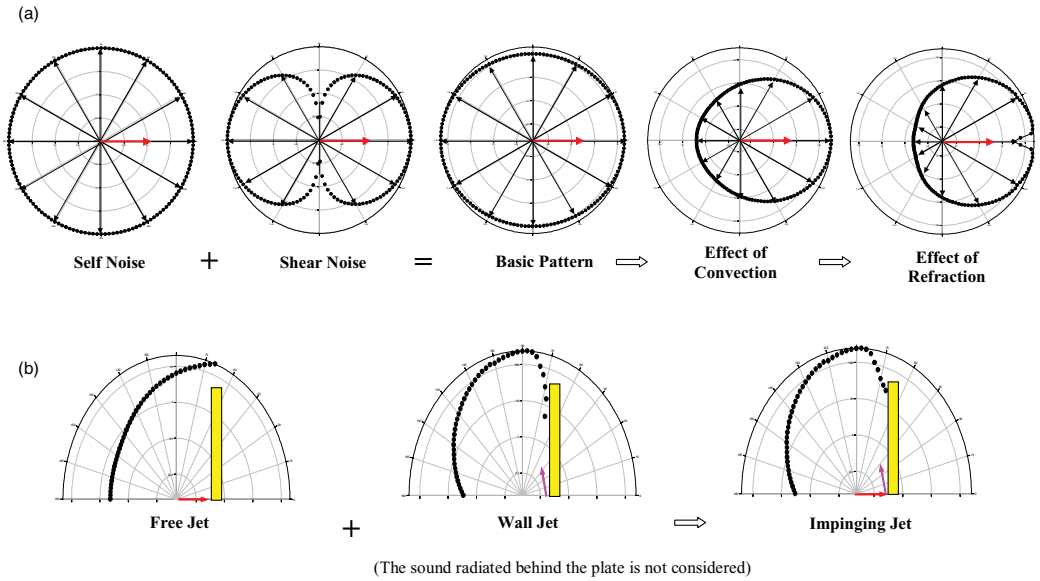

FIG. 19. Directivity pattern. (a) Jet noise. (b) Impinging jet noise.

tones, amplitude of broad band noise decreases with roughness as shown in Fig. 23(b). The increase or decrease in the impinging tone frequency and amplitude may be depends on the impingement bubble size. A smaller impingement bubble size may lead to a reduction in strength of the upstream-propagating acoustic waves, which are in turn responsible for the feedback loop. This could be the cause of change in tonal amplitude. However, advanced flow diagnostics and sophisticated flow visualization techniques are required to confirm this conjecture. In order to explain the reduction in turbulent noise, wall-jet velocity measurement is performed and discussed in Subsection IV B.

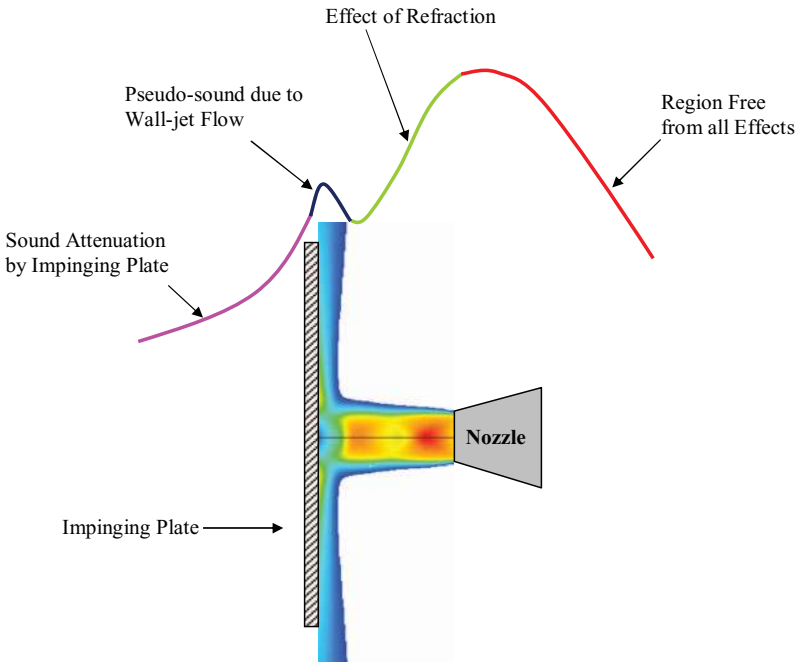

FIG. 20. Sound pressure level directivity pattern of impinging jet.

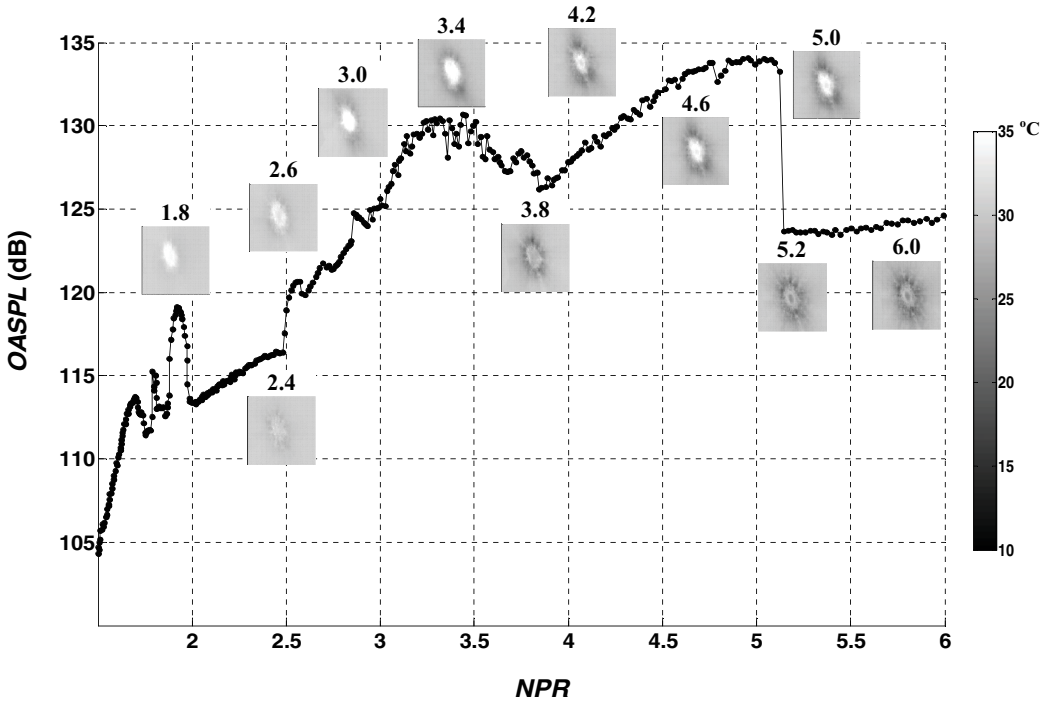

FIG. 21. Variation of temperature at stagnation region and *OASPL* with respect to *NPR* for 36 Grit roughness at $h/d = 5.0$.

B. Wall-jet velocity measurement

In Sec. IV A, temperature measurement shows that roughness of plate changes the characteristics of the stagnation region, and therefore, the amplitude and frequency of the tones. However, even in the absence of tones, roughness leads to reduction in noise, possibly due to the influence of the wall-jet. In order to investigate this, the wall-jet velocity profiles are measured for various *NPR* and roughness values. The wall-jet velocity profile at $r/d = 10$ is obtained with the help of a pitot tube survey along the z-axis, as shown in Fig. 3. This test is performed for all rough surfaces mentioned in Table III for different *NPR* and $h/d = 3$, 4, and 5. It is observed from Fig. 24 that the average velocity at $r/d = 10$ increases as *NPR* increases and results for the plates not shown in Fig. 24 are similar. The velocity profile on the rough plate [Fig. 24(b)] is flatter than that on the smooth plate

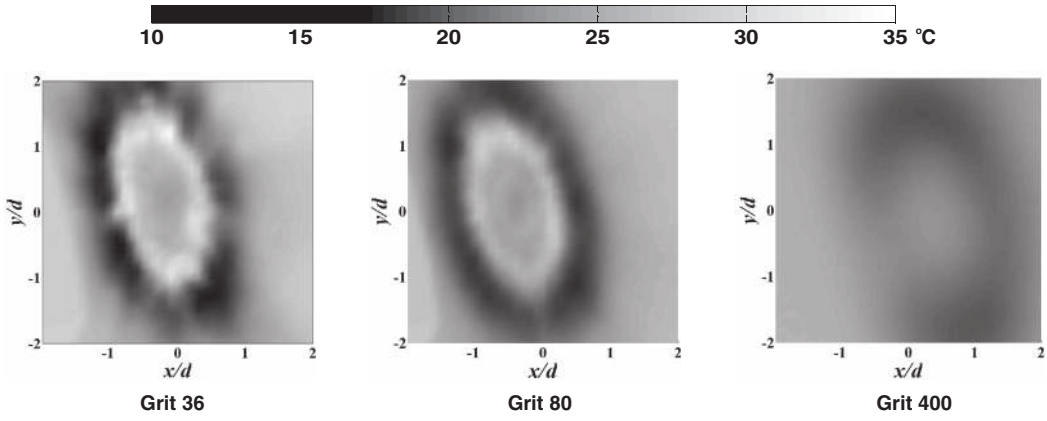

FIG. 22. Temperature contours for jet impinging on different surface roughness plate with $h/d = 3.0$ and $NPR = 3.0$.

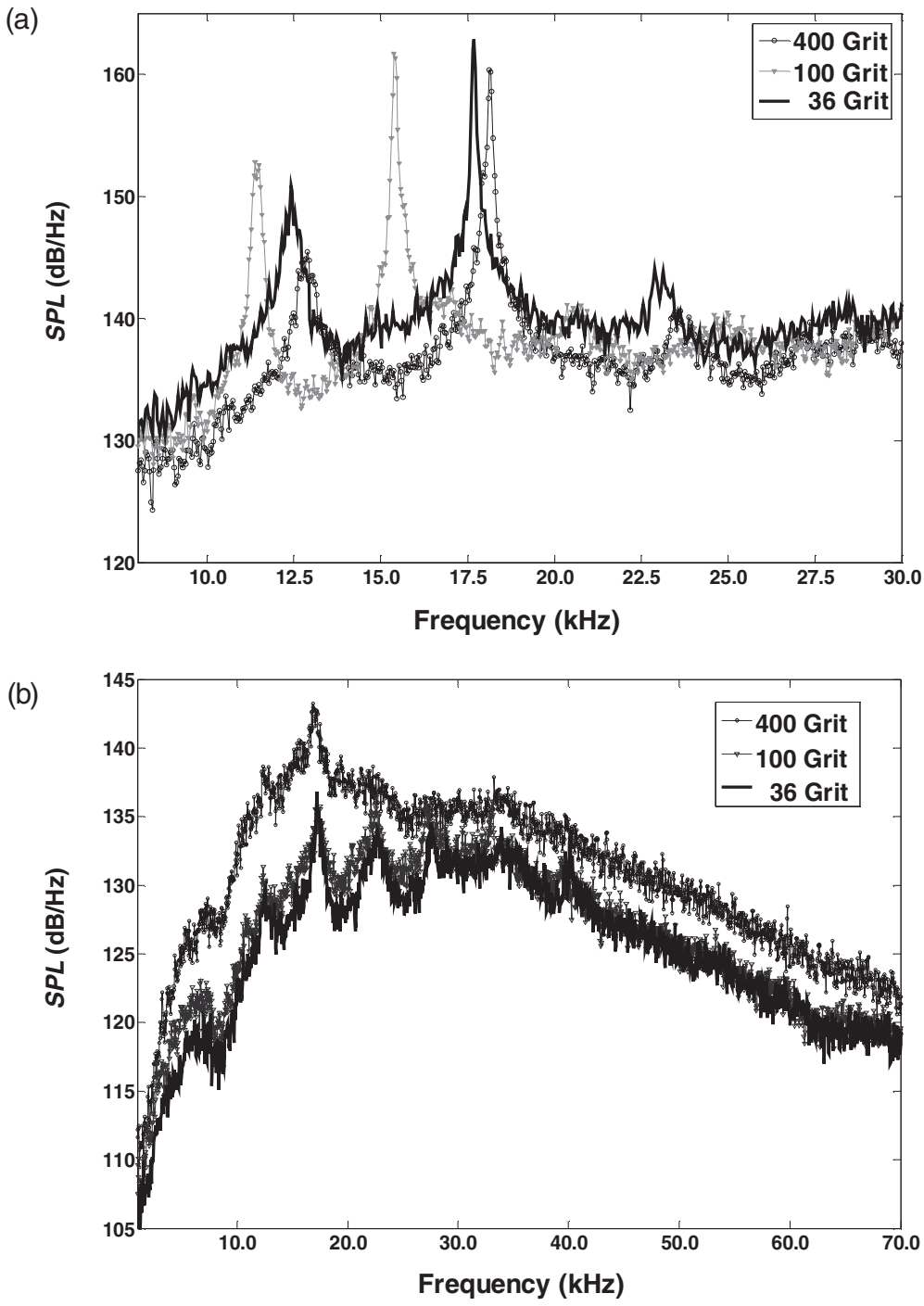

FIG. 23. Spectra comparison for jet impinging on different surface roughness plate with (a) $h/d = 3.0$ and $NPR = 3.0$ and (b) $h/d = 3.0$ and $NPR = 4.0$.

[Fig. 24(a)]. It is found that all these velocity profiles collapse into a single profile, when the velocity is normalised with maximum velocity, U_m (Fig. 25).

Further investigation is done by comparing the maximum velocity in the profile at $r/d = 10$ for all surfaces. Maximum velocity is higher for smooth surfaces compared to rough surfaces, as shown in Fig. 26. This difference between the maximum velocities of smooth and rough surfaces increases

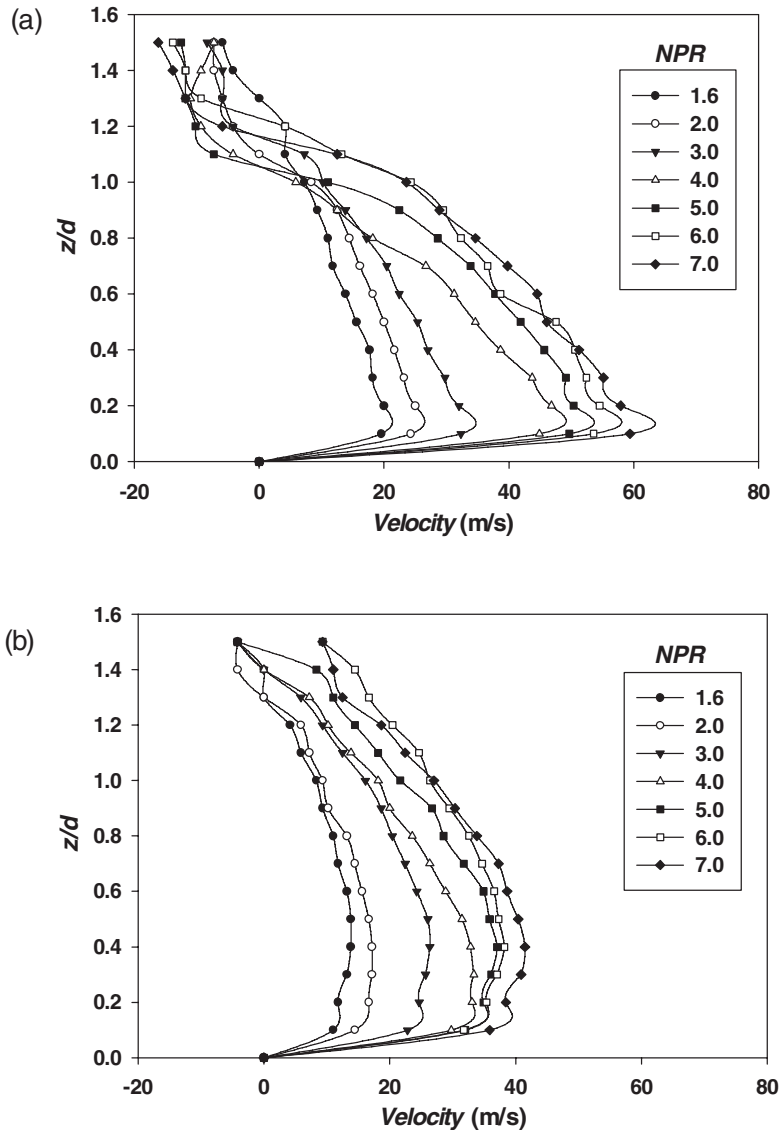

FIG. 24. Velocity distribution at $r/d = 10$ in the radial wall jet for $h/d = 3.0$ for various *NPR* for (a) smooth plate and (b) 36 Grit surface.

monotonically with *NPR*. These trends are in agreement with the results of Tu and Wood.[59] Similar results were also observed by Blake for turbulent boundary layer, mean velocity decreases with roughness.[60]

The reduction of maximum velocity and average velocity due to surface roughness leads to a decrease in acoustic power. It is also seen that even after the removal of tones from a signal, the directivity pattern remains the same for all the roughness (Fig. 16). This may be attributed to the decrease in the mean velocity that affects the shear noise.[61] In the literature, it is seen that the noise generated by rough surface is higher than that generated by smooth surface for very low speeds and it is in agreement with theory. However, for high speed flows, the results are contradictory. The cause of noise reduction in rough surfaces is the reduction of mean velocity by the rough surface. The radiated acoustic power for jet is given as (Blake)[61]

$$AP = \frac{1}{c^5}\left\{\int_0^{\pi} (M_c \cos\theta)^{-5} \sin\theta d\theta\right\} \rho_o U_j^8 d^2 f_1(R_d, M_c). \quad (4)$$

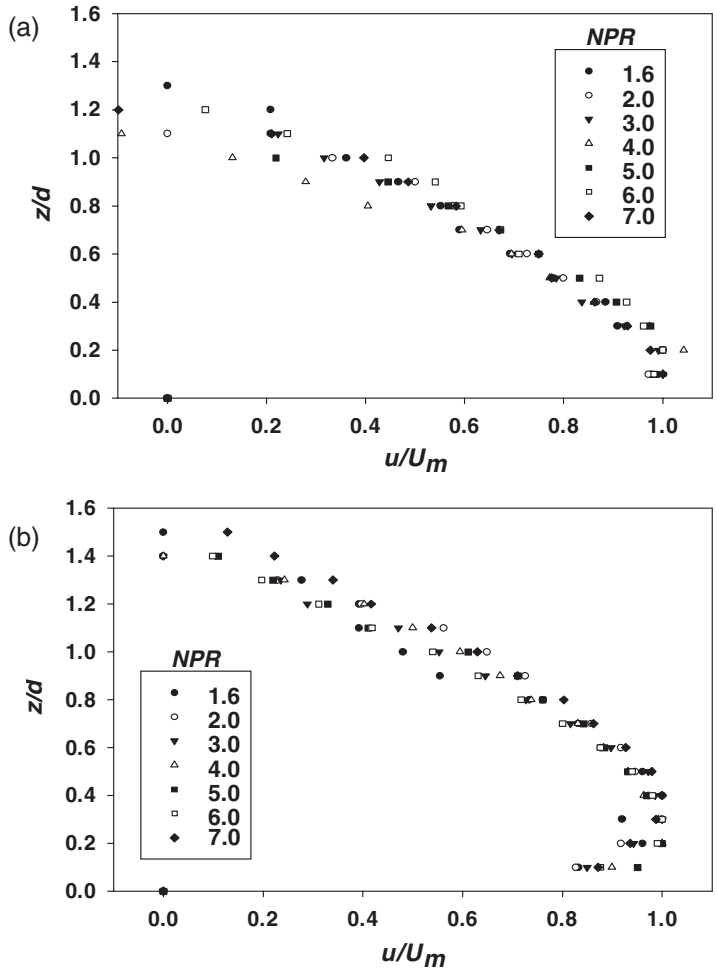

FIG. 25. Dimensionless velocity distribution in the radial wall jet produced by an impinging jet at $h/d = 3.0$ for (a) smooth plate and (b) 36 Grit surface.

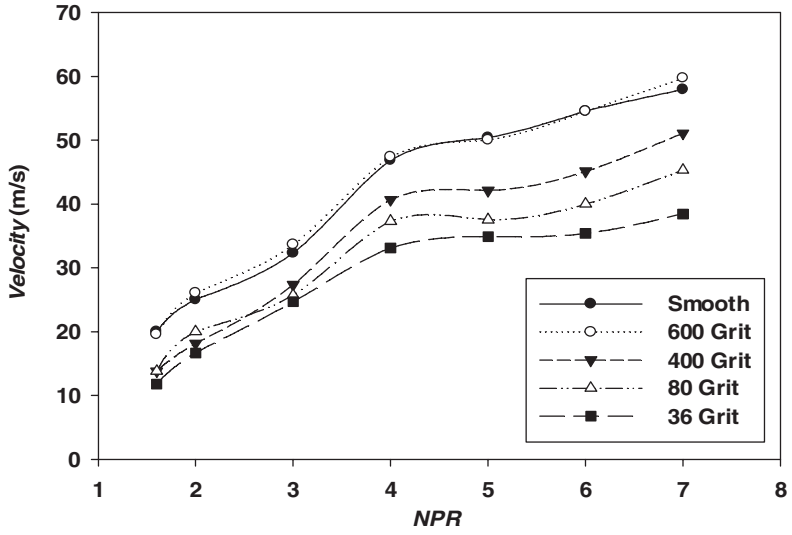

FIG. 26. Comparison of maximum velocity at $r/d = 10$ and $h/d = 3.0$ for different plate surface roughness.

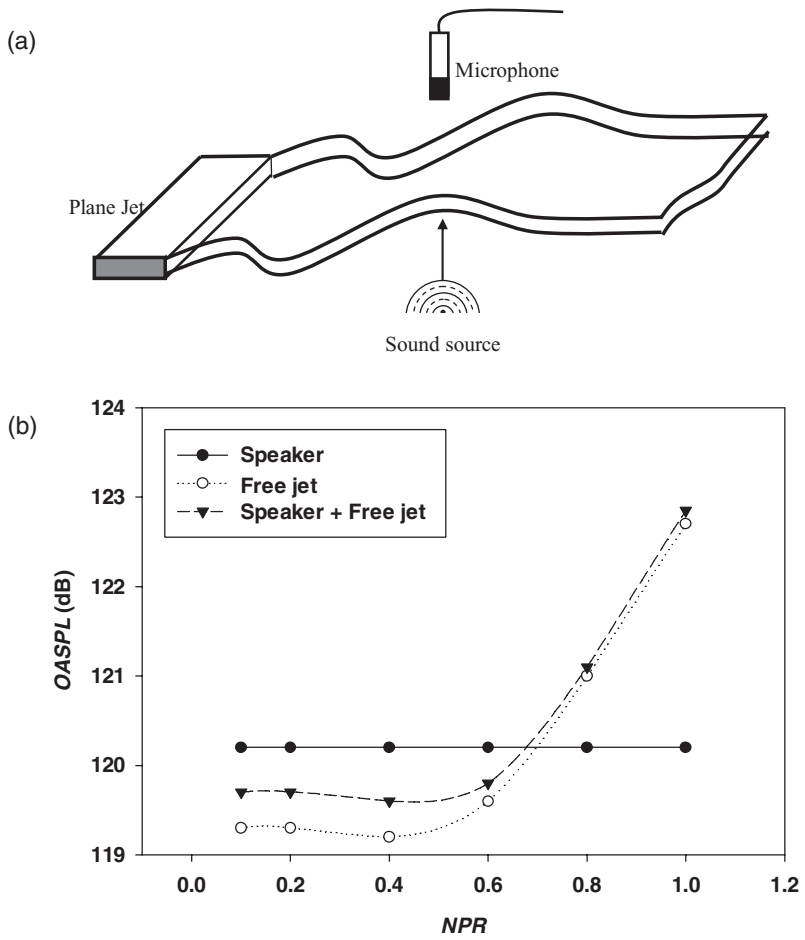

FIG. 27. Effect of velocity on sound propagation. (a) Experimental setup. (b) Results indicating the reduction of sound intensity due to the flow barrier.

In above equation d, ρ_o, and U_j, are jet diameter, air density, and jet mean velocity, respectively, and R_d is Reynolds number with characteristic length as jet diameter. Function f_1 incorporates the dependence of acoustic power on Reynolds number and Mach number.

Therefore, for a high speed impinging jet the radiated acoustic part can be written as

$$AP = \frac{1}{c^5}\left\{\int_0^{\pi}(1 - M_c\cos\theta)^{-5}\sin\theta d\theta\right\}\rho_o U_j^8 d^2 f_2\left(R_d, M_c, h/d\right) + \frac{1}{c^5}\left\{\int_0^{\pi}(1 - M_c\cos\theta)^{-5}\sin\theta d\theta\right\}\rho_o U_{wj}^8 d^2 f_3\left(R_d, M_c, h/d\right), \quad (5)$$

where U_{wj} is the wall-jet mean velocity and functions f_2 and f_3 incorporate the dependence of acoustic power on Reynolds number, Mach number, and the nozzle-plate spacing.

In the case of effect of roughness of impinging plate keeping other parameter constant and neglecting nonlinearities involved due to the presence of feedback loop, it can be written as

$$AP \propto U_{wj}^8. \quad (6)$$

Thus, from the present experiments, it may be concluded that roughness causes the mean velocity of wall-jet to decrease, thereby reducing the acoustic power of jet impingement noise.

C. Effect of noise source shielding by the wall-jet shear layer

In order to investigate the effect of wind speed, a simple experiment is carried out using a plane jet and a speaker, arranged as shown in Fig. 27(a). The speaker and the microphone are placed inline, on either sides of a plane jet. Sound generated by the speaker, plane jet, operated individually and together, is measured by the microphone. Experiments are performed at various velocities of the plane jet. Figure 27(b) indicates that the presence of the plane jet reduces the noise of speaker propagated across the plane jet. The shear layer between the speaker and microphone masks the sound by shielding and refraction mechanisms. These effects are more dominant at high speeds. The same phenomenon is observed in a wall-jet. When the jet impinges on the rough surface it produces more noise and heat transfer by friction than on a smooth surface, resulting in reduction of wall-jet mean velocity. However, this noise is masked inside the shear layer and the reduction of mean velocity results in lowering the shear noise produced by wall-jet.

V. CONCLUSION

A detailed acoustic, flow and thermal investigation of the impinging jet are conducted by varying parameters such as roughness of impinging surface ($0.063 \leq R_a \leq 125.5$), nozzle pressure ratio ($1.4 \leq NPR \leq 6.0$), and distance between jet exit and impinging plate ($1 \leq h/d \leq 10$). Experimental acoustic data are validated using multimode screech and impinging tonal frequency formulae. Wall jet velocity results are validated using power law. Directivity study is performed for distribution of acoustic radiation around the impinging jet system and to measure total acoustic power. Blow down study is performed by varying impinging plate roughness and stand-off distance to investigate the effect of nozzle pressure ratio. The results indicate that roughness of impingement plate widens the staging region of impingement noise. In general, rough surfaces produce less noise than smooth surfaces and toneless spectra confirm that roughness leads to lower levels of turbulent noise even in case of staging region. Smooth surfaces generate higher levels of tonal noise than rough surfaces. The staging region is characterized by ups and downs of *OASPL* values due to the mode switching of tones and this is confirmed by phase difference using three microphones placed normal to each other at the jet exit plane. Acoustic power of impinging jets with tones are comparable, while the acoustic power of tone-less cases monotonically decrease with increasing surface roughness. The impinging jet directivity is constructed from the directivity patterns of free jet and wall-jet. Thermal imaging in the stagnation region indicates that whenever the tone is present, the temperature at the stagnation region is high. The cause of noise reduction in the case of rough impingement plates is due to the reduction of maximum velocity and average velocity in the wall jet. The shear layer masks the noise sources inside, leading to noise attenuation, as demonstrated by a separate experiment.

ACKNOWLEDGMENTS

The authors are grateful to the anonymous reviewers for their valuable comments and suggestions that immensely helped improve the paper.

[1] A. Powell, "On the mechanism of chocked jet," Proc. Phys. Sec. London, Sect. B **66**, 1039–1057 (1953).
[2] W. Konig, "Zur Theorie der Schneidentone," Phys. Z. **13**, 1053–1055 (1912).
[3] A. Powell, "On the edgetone," J. Acoust. Soc. Am. **33**, 395–409 (1961).
[4] N. Curle, "The mechanics of edgetones," Proc. R. Soc. London, Ser. A **216**, 412–424 (1953).
[5] A. Marsh, "Noise measurements around a subsonic air jet impinging on a plane rigid surface," J. Acoust. Soc. Am. **33**, 1065–1066 (1961).
[6] K. A. Mørch, "A theory for the mode of operation of the Hartmann air jet generator," J. Fluid Mech. **20**, 141–159 (1964).
[7] L. F. Henderson, "Experiments on the impingement of a supersonic jet on a flat plate," J. Appl. Math. Phys. **17**, 553–569 (1966).
[8] F. R. Wagner, "The sound and flow field of an axially symmetric free jet upon impact on a wall," NASA TT F-13942, 1971.
[9] T. Nakatogawa, M. Hirata, and Y. Kukita, "Disintegration of a supersonic jet impinging normally on a flat plate," J. Spacecr. Rockets **8**(4), 410–411 (1971).
[10] O. I. Gubanova, V. V. Lunev, and L. I. Plastinina, "The central break-way zone with interaction between a supersonic underexpanded jet and a barrier," Fluid Dyn. **6**, 298–301 (1973).
[11] G. Neuwerth, "Acoustic feedback phenomena of the subsonic and hypersonic free jet impinging on a foreign body," NASA TT F-15, 719, 1974.

[12] B. G. Semiletenko, B. N. Sobkolov, and V. N. Uskov,"Features of unstable interaction between a supersonic jet and infinite baffle," Fluid Mech.-Sov. Res. **3**(1), 90–95 (1974).
[13] A. M. Petrie, "An experimental investigation of the noise produced by air jet impingement on flat plates," Appl. Acoust. **7**(2), 117–126 (1974).
[14] C. M. Ho and N. S. Nossier, "Dynamics of an impinging jet. Part 1. The feedback phenomenon," J. Fluid Mech. **105**, 119–142 (1981).
[15] A. Powell, "The sound-producing oscillations of round under-expanded jets impinging on normal plates," J. Acoust. Soc. Am. **83**, 515–533 (1988).
[16] T. D. Norum, "Ground impingement of supersonic jets from nozzles with various exit geometries," J. Aircr. **29**(6), 993–998 (1992).
[17] C. D. Donaldson and R. S. Snedeker, "A study of free jet impingement. I. Mean properties of free and impinging jets," J. Fluid Mech. **45**, 281–319 (1971).
[18] J. Crafton, E. Cambell, E. J. Sulliavan, and G. Elliot, "Pressure measurements on the impingement surface of sonic and sub-sonic jets impinging onto a flat plate at inclined angles," Exp. Fluids **40**(5), 697–707 (2006).
[19] E. I. Sokolov and I. V. Shatalov, "Influence of viscosity on the flow in the circulation region in front of a flat obstacle perpendicular to the axis of a supersonic under-expanded jet," Izv. Akad. Nauk SSSR, Mekh. Zhidk. Gaza **3**, 47–52 (1981).
[20] B. Henderson, "The connection between sound production and jet structure of the supersonic impinging jet," J. Acoust. Soc. Am. **111**, 735–747 (2002).
[21] J. C. Carling and B. L. Hunt, "The near wall jet of a normally impinging, uniform, axis-symmetric, supersonic jet," J. Fluid Mech. **66**, 159–176 (1974).
[22] A. G. Golubkov, B. K. Koz'menko, V. A. Ostapenko, and A. V. Solotchin, "On the interaction of an underexpanded supersonic jet with a finite flat baffle," Fluid Mech.-Sov. Res. **3**, 96–102 (1974).
[23] J. H. Gummer and B. L. Hunt, "The impingement of non-uniform, axisymmetric supersonic jets on a perpendicular flat plate," Isr. J. Technol. **12**, 221–235 (1974).
[24] I. P. Ginzburg, V. N. Semiletenko, and V. N. Uskov,"Experimental study of underexpanded jets impinging normally on a plane baffle," Fluid Mech.-Sov. Res. **4**(3), 93–105 (1975).
[25] V. N. Glaznev, V. S. Demin, and A. M. Yakushev, "Self-oscillations in an underexpanded jet flowing into a barrier," Fluid Dyn. **12**(6), 848–852 (1977).
[26] H. L. Back and V. Sarohia, "Pressure pulsations on a flat plate normal to an underexpanded jet,"AIAA J. **16**(6), 634–636 (1978).
[27] P. J. Lamont and B. L. Hunt, "The impingement of underexpanded, axisymmetric jets on perpendicular and inclined flat plates," J. Fluid Mech. **100**, 471–511 (1980).
[28] A. Krothapalli, "Discrete tones generated by an impinging underexpanded rectangular jet," AIAA J. **23**, 1910–1915 (1985).
[29] J. Iwamoto and B. E. L. Deckker, "Development of flow field when a symmetrical underexpanded sonic jet impinges on a flat plate," J. Fluid Mech. **113**, 299–313 (1981).
[30] B. Henderson and A. Powell, "Experiments concerning tones produced by an axisymmetic choked jet impinging on a flat plate," J. Sound Vib. **168**(2), 307–326 (1993).
[31] R. W. Wlezien, and P. J. Ferraro, "Aeroacoustic environment of an advanced short takeoff and vertical landing aircraft in hover," AIAA J. **30**(11), 2606–2612 (1992).
[32] N. L. Messersmith, "Aeroacoustics of supersonic and sonic impinging jets," AIAA Paper No. 95-0509, 1995.
[33] D. B. Levin and D. A. Wardwell, "Single jet-induced effects on small-scale hover data in ground effect," J. Aircr. **34**, 400–407 (1997).
[34] A. Krothapalli, E. Rajkuperan, F. Alvi, and L. Lourenco,"Flow field noise characteristics of a supersonic impinging jet," J. Fluid Mech. **392**, 155–181 (1999).
[35] F. S. Alvi and K. G. Iyer, "Mean and unsteady flow field properties of supersonic impinging jets with lift plates," AIAA Paper No. 99-1829, 1999.
[36] F. S. Alvi, C. Shih, R. Elavarasan, G. Garg and K. Krothapalli "Control of supersonic impinging jet flows using supersonic microjets," AIAA J. **41**(7), 1347–1355 (2003).
[37] A. Krothapalli, R. Elavarasan, L. Venkatakrishnan, and L. Lourenco, "Suppression of self- sustained oscillations in a supersonic impinging jet," AIAA J. **39**(12), 2366–2373 (2001).
[38] Z. Travnicek and V. Tesar, "Annular synthetic jet used for impinging flow mass transfer," Int. J. Heat Mass Transfer **46**(17), 3291–3297 (2003).
[39] B. Henderson, J. Bridges, and M. Wernet, "An experimental study of the oscillatory flow structure of tone-producing supersonic impinging jets," J. Fluid Mech. **542**, 115–137 (2005).
[40] S. I. Kim and S. O. Park, "Oscillatory behavior of supersonic impinging jet flows," Shock Waves **14**(4), 259–272 (2005).
[41] R. Kumar, S. Lazic, and F. S. Alvi, "Active control of high temperature supersonic impinging jets," AIAA Paper 2008-360, 2008.
[42] K. A. Phalnikar, R. Kumar, and F. S. Alvi, "Experiments on free and impinging supersonic microjets," Exp. Fluids **44**(5), 819–830 (2008).
[43] A. M. Md. Ashraful, S. Matsuo, and T. Setoguchi, "Supersonic moist air jet impingements on flat surface," J. Therm. Sci. **19**(1), 51–59 (2010).
[44] M. S. Howe, "On the generation of sound by turbulent boundary layer flow over a rough wall," Proc. R. Soc. London, Ser. A **395**, 247–263 (1984).
[45] M. S. Howe, "The influence of viscous surface stress on the production of sound by turbulent boundary layer flow over a rough wall," J. Sound Vib. **104**(1), 29–39 (1986).
[46] M. J. Lighthill, "On sound generated aerodynamically. I. General theory," Proc. R. Soc. London, Ser. A **211**(1107), 564–587 (1952).

[47] C. K. W. Tam, "Intensity, spectrum, and directivity of turbulent boundary layer noise," J. Acoust. Soc. Am. **57**(1), 25–34 (1975).
[48] M. S. Howe, "Sound produced by turbulent boundary layer flow over a finite region of wall roughness, and over a forward facing step," J. Fluids Struct. **3**, 83–96 (1989).
[49] A. V. Smol'yakov, "Noise of a turbulent boundary layer flow over smooth and rough plates at low mach numbers," Acoust. Phys. **47**(2), 218–225 (2001).
[50] A. S. Hersh, "Surface roughness generated flow noise," AIAA Paper No. 83-0786, 1983.
[51] T. J. S. Jothi and K. Srinivasan, "Role of initial conditions on noise from underexpanded pipe jets," Phys. Fluids **21**, 066103-1–066103-17 (2009).
[52] A. Meslem, V. Sobolik, F. Bode, K. Sodjavi, Y. Zaouali, I. Nastase, and C. Croitoru, "Flow dynamics and mass transfer in impinging circular jet at low Reynolds number. Comparison of convergent and orifice nozzles," Int. J. Heat Mass Transfer **67**, 25–45 (2013).
[53] J. H. Gao and X. D. Li, "A numerical study of nozzle boundary layer thickness on axisymmetric supersonic jet screech tones," *12th AIAA/CEAS Aeroacoustics Conference (27th AIAA Aeroacoustics Conference)*, Cambridge, Massachusetts, 8–10 May 2006.
[54] W. R. Quinn and G. F. Marsters, "Upstream influence on turbulent jet from cruciform nozzles," Aeronaut. J. **89**(882), 55–58 (1985).
[55] M. Yaga, Y. Kinjo, M. Tamashiro, and K. Oyakawa,"Flow characteristics of rectangular underexpanded impinging jets," J. Therm. Sci. **15**(1), 59–64 (2006).
[56] J. H. Gao and X. D. Li, "A multi-mode screech frequency prediction formula for circular supersonic jets," J. Acoust. Soc. Am. **127**(3), 1251–1257 (2010).
[57] J. B. R. Loureiro and A. P. Silva Freire, "Wall shear stress measurements and parametric analysis of impinging wall jets," Int. J. Heat Mass Transfer **55**, 6400–6409 (2012).
[58] H. S. Ribner, "Quadrupole correlations governing the pattern of jet noise," J. Fluid Mech. **38**(1), 1–24 (1969).
[59] C. V. Tu and D. H. Wood, "Wall pressure and shear stress measurements beneath an impinging jet," Exp. Therm. Fluid Sci. **13**(4), 364–373 (1996).
[60] W. K. Blake, "Turbulent boundary-layer wall-pressure fluctuations on smooth and rough walls," J. Fluid Mech. **44**(4), 637–660 (1970).
[61] W. K. Blake, *Mechanics of Flow-Induced Sound and Vibration*, General Concepts and Elementary Sources Vol. I (Academic Press, Inc., New York, 1986), p. 179.